CHAPTER

3

Remote Sensing of Aerosols From Space: Retrieval of Properties and Applications

Alaa Mhawish, Manish Kumar*, Akhila K. Mishra†, Prashant K. Srivastava*, Tirthankar Banerjee***

***Institute of Environment and Sustainable Development, Banaras Hindu University, Varanasi, India**
†Indian Institute of Remote Sensing, Dehradun, India

1 INTRODUCTION

The use of earth-observing satellites in air-quality management is although contemporary, but first began nearly four decades ago. In the late 1970s, satellite imagery from the GOES and Landsat satellites was utilized to identify haze (Lyons and Husar, 1976) and study population exposure to air pollution (Todd et al., 1979). However, the advanced scientific tools for sharing and using satellite data have improved the potential of satellite-retrieved information to be used for assessment, forecasting, and management of air quality. The concurrence of satellite and ground-based information is now widely accepted for urban-scale air-quality management among both the scientific and the policy-making communities. The most remarkable feature in applying satellite-derived information enlists the downscaling of synoptic and geospatial information to assess localized phenomena. The foremost applications include the measurement of gaseous pollutants, like ozone (O_3), sulfur dioxide (SO_2), nitrogen dioxide (NO_2), carbon monoxide (CO), formaldehydes (HCHO), etc. Airborne particulates are also well explored by satellite remote sensing due to their relevance to climate science, heterogeneous nature, and spatial variability. Fraser et al. (1984) for the first time accomplished successful retrieval of aerosol optical depth (AOD) using GOES observations over land and applied it to inspect a haze episode over the eastern United States. A sharp rise in aerosol remote-sensing information over the last decade has been observed and has been utilized in multiple ways including the estimation of ground-level aerosols (Dey et al., 2012), mortality studies (Hu, 2009; Corbett et al., 2007), crop simulations (Fang et al., 2011), identification of extreme

Remote Sensing of Aerosols, Clouds, and Precipitation
https://doi.org/10.1016/B978-0-12-810437-8.00003-7

events (Kumar et al., 2014) and for air-quality forecasting (Kumar et al., 2007). These multifaceted applications of remote-sensing technology have opened up a wide scope for interdisciplinary interventions in air-quality studies.

The management of near-surface air quality is essential due to its possible implications for public health, agricultural output, visibility, and aesthetic and cultural values. However, the intricacy in the availability of ground-based data makes the entire process of air-quality management difficult and uneconomic. Satellite-based observations reduce uncertainties in spatial distribution of air pollutants and the associated phenomena affecting them over synoptic and geospatial context. The estimation of ground-level pollutant concentration using space-based observations is one of the foremost applications of remote sensing, which has recently been used for air-quality management. Near-surface aerosols with highly heterogeneous behavior are being analyzed on various scales and resolutions using satellite-based observations. Researchers have exploited the dependence of aerosol optical properties on their size distributions for estimating near-surface concentrations. Improved associations were further assessed by Wang and Christopher (2003) between AOD and $PM_{2.5}$ in Alabama. However, such a relationship is highly region-specific and depends on various meteorological conditions. These assessments made a firm basis for the development of empirical relationships between satellite-derived properties and their ground-based counterparts. Studies reported the improved relationship between MODIS-derived AOD and near-surface $PM_{2.5}$ with a specific set of circumstances, including cloud-free conditions, low boundary layer heights, low relative humidity and with high aerosol loadings (Gupta et al., 2007). Additionally, the inclusion of time varying meteorological variables along with the chemistry transport model are reported to further improve the relationship.

Most of the epidemiological studies rely on near-surface measurements of air pollutants as human beings are subject to the toxicity of pollutants, most of which are present at the breathing level. However, sparse monitoring networks limit the applicability of surface-measured pollutant concentrations for exposure studies (Kumar et al., 2015a). Spatially resolved estimates of particulate matter using satellite AOD provide a better scope for assessing pollution-induced diseases and mortality. Hu (2009), using a geographically weighted regression derived near surface $PM_{2.5}$ concentrations in the eastern United States, inferred a significant hike in coronary diseases with an increase in $PM_{2.5}$. Using geospatial emission inventories, Corbett et al. (2007) revealed the mortality due to shipping-related particulate emissions. Evans et al. (2013) found distinctly high mortality estimates from satellite observations in comparison to the ground-based databases. However, considerable collinearity was observed between satellite-derived mortality estimates and chemical transport model simulations. Thus the regions with high susceptibility to diseases induced by air pollution may be conveniently mapped using remote sensing and geographic information systems (GIS) techniques, leading to the formulation of suitable mitigation plans. These techniques have been successfully implemented in different parts of the world.

The appropriateness of any air-quality management plan requires precise information about emission inventories, considering information on particulate sources, emission strengths, and rates (Banerjee et al., 2011). Satellite-based measurements of various aerosol products are extensively used to examine possible sources and to develop a spatial emission map. Additionally, with the advancement of remote-sensing observation in the last decades, techniques have been developed for using these observations as constraints on pollutant sources.

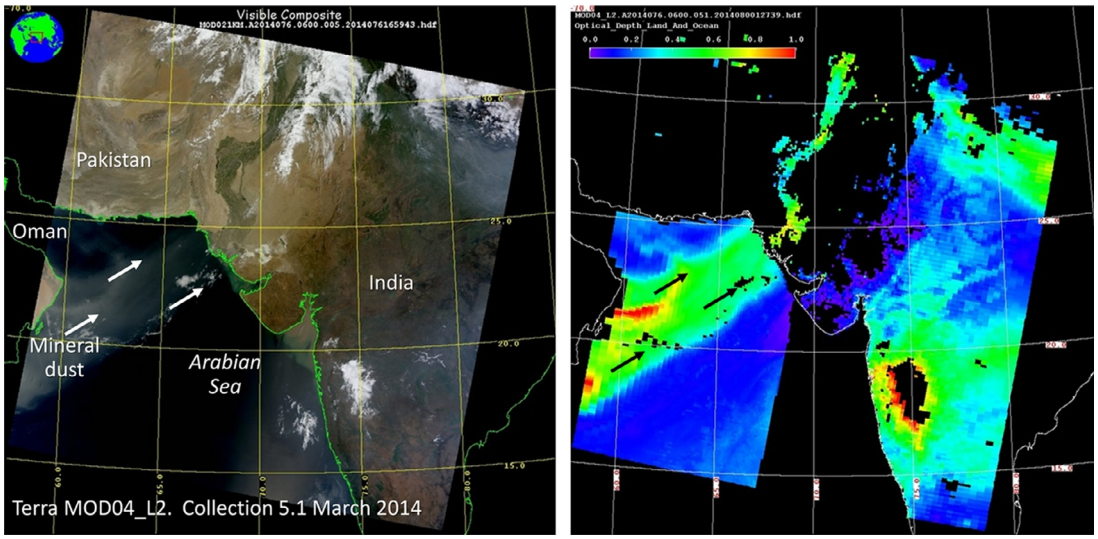

FIG. 1 Transboundary movement of mineral dust over South Asia. *Note*: Both true color and AOD images are courtesy of Terra MODIS. *Modified from Kumar, M., Tiwari, S., Murari, V., Singh, A.K., Banerjee, T., 2015b. Wintertime characteristics of aerosols at middle Indo-Gangetic plain: impacts of regional meteorology and long range transport. Atmos. Environ. 104, 162–175.*

Likewise, during summer and premonsoon months, the transboundary movement of airborne particulates originating in Middle East dry regions often causes dust storms over the Indian subcontinent (Fig. 1). Inverse modeling of MODIS AOD in conjunction with a few advanced models such as GOCART have been utilized by Dubovik et al. (2007) for the quantification of major aerosol sources. Wang et al. (2013) combined satellite-measured radiances and inverse modeling to spatially constrain sources of dust emissions in the Taklimakan and Gobi deserts. Wang et al. (2016) also reported a new approach to integrate OMI-retrieved SO_2 measurements and GEOS-Chem adjoint model simulations to constrain anthropogenic emissions of SO_2. Spatially resolved information on backscatter characteristics and classified aerosol types retrieved through the CALIPSO satellite constructively helps in apportioning its sources. Mazzoni et al (2007) determined the heights of smoke plumes from wildfires through MISR retrievals. Not limited to aerosols, MODIS and MISR aerosol products were also interpreted for annual growth rates of sulfur emissions over China (van Donkelaar et al., 2008).

The framework for managing air quality for a regional or national interest includes a forecasting mechanism that can take care of future emission scenarios and anticipated risks associated with it. Recent advancements in remote-sensing bring promising support to air-quality forecasting. Assessments of satellite imagery of smoke from MODIS, AIRS, and other fire detection maps are being made with the help of GIS to project the effects of wildfire and biomass burning. There are some specific web tools that collect all relevant information together, such as Infusing Satellite Data into Environmental Applications (IDEA) and the Hazard Mapping System Fire and Smoke Product (HMS). Also, some extreme events including dust storms, haze episodes, and smog become a serious nuisance to the regional air quality, affecting health, visibility, and climate. Several remote-sensing techniques

have been documented in studies, which could help air-quality managers in minimizing risks associated with such extreme events.

Satellite remote sensing of aerosols does have some limitations. Technical and scientific issues such as cloud contamination, surface reflectance, sensitivity of instruments, and other atmospheric errors need to be considered while using remote-sensing techniques for atmospheric and climate science. Many satellites have passive sensors that are used to retrieve optical properties only during daytime and for the entire column, which may not be relevant to ground-level concentrations. Retrieving aerosol optical properties becomes additionally complicated due to real-time variations in aerosol microphysical properties influenced by existing meteorology and the source profile. Therefore, real-time measurement of aerosol properties always remains a challenge. Additionally, complexity in data retrieval methods, data access, and a low level of understanding from policymakers about the satellite data put limitations on its use. Resolution—be it spatial, spectral, temporal, or radiometric—regulates the applicability of a particular data product, but often there is a tradeoff between these. Likewise, polar-orbiting satellites offer higher resolution with less-frequent global coverage while geostationary satellites have lower resolution but almost daily global coverage. Therefore, often satellite data products are application-specific and the user should consider the limitations/quality of data products before the intended use.

2 AEROSOLS: HETEROGENEITY AND CLIMATIC IMPLICATIONS

The climate-governing properties of atmospheric aerosols have been well acknowledged (Ramana et al., 2010; Schwartz and Andreae, 1996; Hansen et al., 1997; Banerjee et al., 2017a). The complex aerosol chemistry mediated through its surface additionally supports multifaceted climatic implications. Among various atmospheric entities, aerosols constitute a major source of uncertainty in their role in climate perturbations mainly due to the associated heterogeneities (Murari et al., 2015).

The degree of heterogeneity in aerosol properties highly depends on geological and topographical features (Ramanathan and Ramana, 2005), source strengths, and meteorological factors (Banerjee et al., 2015). The complicacy in aerosol-climate interaction is governed by its multidimensional heterogeneity, mainly in space, time, chemical composition, size distribution, sources, vertical distribution, and mixing states, leading to different climatic impacts (Fig. 2).

A wide range of spatial heterogeneity has been reported in the global distribution of aerosols, which is responsible for the differential climatic impacts (van Donkelaar et al., 2015). Owing to their lower atmospheric residence time (typically hours to a few weeks), the distribution of aerosols often remains in proximity to their sources. Additionally, local geography and meteorology are the most influential factors in regulating aerosol properties. Therefore, often the global distribution of aerosol loading is specifically linked with isolated geographical regions. Likewise, some of the major recognized regions—typically called aerosol hotspots—are tropical Africa, Eastern China, the Indo-Gangetic Plain (IGP) of South Asia, the tropical region of Central America, Southeast Asia, and Mexico. Fig. 3 depicts the global distribution of columnar AOD (Fig. 3A) and fine-mode fractions (Fig. 3B) retrieved from the Terra-MODIS satellite for August 2015. The heterogeneity in aerosol optical and microphysical properties over a wide range of spatial and temporal scales obstructs the true estimates of aerosol-induced climate change. Likewise, the Sahara Desert in Northern Africa is fairly characterized by coarser mineral dusts (Jiménez et al., 2010) while the Southeast Asian region is typically dominated by secondary aerosols (Trivitayanurak et al., 2012). Singh et al. (2017a) reviewed the predominate sources of airborne

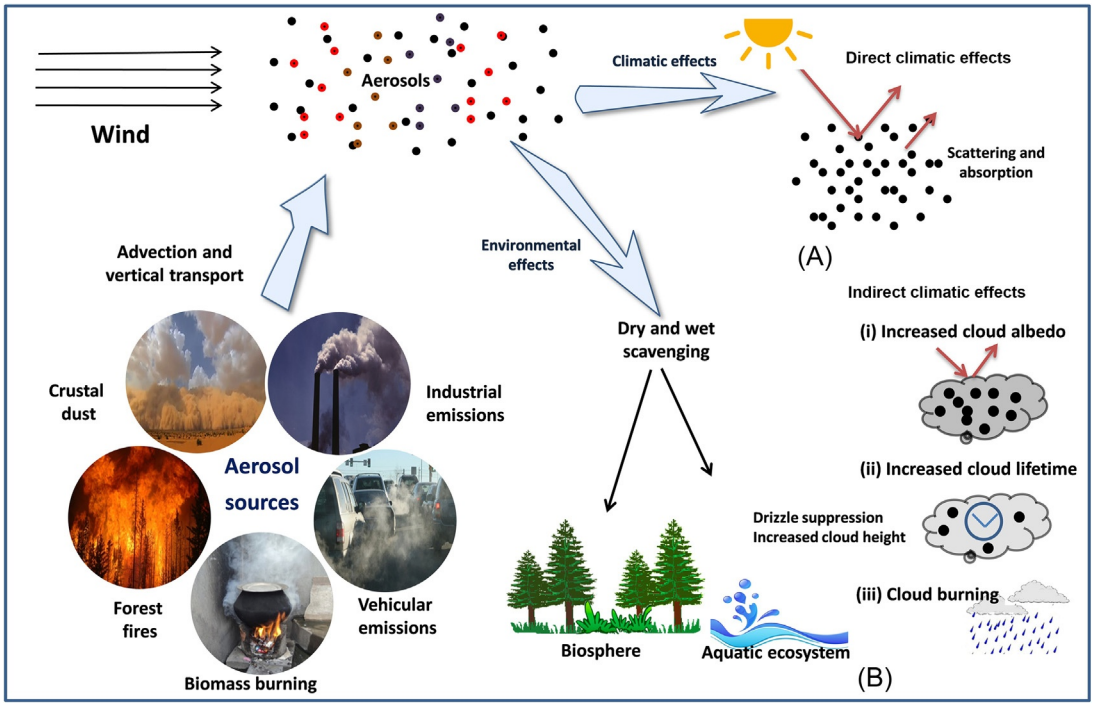

FIG. 2 Aerosol heterogeneity and climate-governing properties.

fine particulates over South Asia and reported significant contributions from vehicular and industrial sources with significant variabilities, both in terms of season and geography. The entire Indo-Gangetic basin in South Asia is characterized with mixed aerosols with dominance of coarser dusts at the upper basin while elevated proportions of finer aerosols and soot over central and lower parts (Fig. 9). Sen et al. (2017) concluded the presence of a very high particulate load, especially over the IGP, which reportedly undergoes long-range transport of aerosols from its source to the Indo-Himalayan Range and Bay of Bengal. Extremely high particulate loadings have also been reported over the middle IGP during winter (Kumar et al., 2015b, 2017a; Sen et al., 2014) while minimal concentrations were observed during monsoon season (Murari et al., 2015, 2017). Das et al. (2014) also observed a seasonality in dust transport in the Indian region with an enhanced dust loading (AOD > 0.5) over the oceans during monsoon season. Efforts were also made to characterize the particulate composition and transport over the IGP. The coarse transported dust from the great Indian Thar and other Middle East countries is rich in iron, calcium, silicon, aluminum, magnesium, lithium, and phosphorus (Moreno et al., 2012). Aerosols emitted from combustion sources such as biomass/refuse burning, forest fires, and vehicular emissions are characterized by soot, black carbon (BC), sulfates, nitrates, and ammonium ions (Murari et al., 2015).

The existence of aerosols in a wide-size spectrum (nm to μm) is another source of heterogeneity that influences the climate and is reported to play a crucial role in cloud microphysical properties. Aerosols of natural origin (mineral dust, sea salt) are usually coarser in size except for sulfate and carbonaceous aerosols, which are emitted from volcanic eruptions and

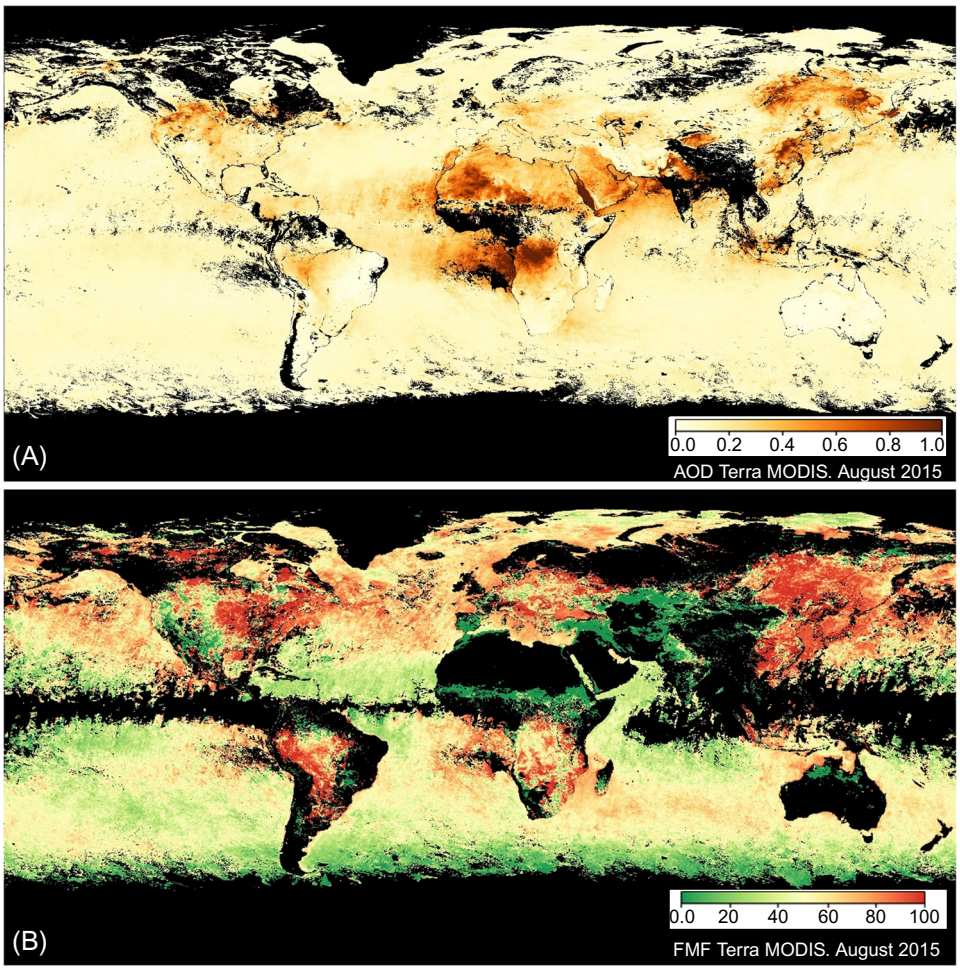

FIG. 3 (A and B) Mean global aerosol loading for August 2015 retrieved from Terra MODIS (A) AOD at 550 nm (B) fine-mode fractions (FMF).

forest fires. In contrast, most of the anthropogenic sources such as vehicular emissions, biomass burning, and fossil-fuel combustion release particulates with dominance of finer particulates. The information on mixing states of aerosols is one of the unresolved issues in atmospheric sciences due to their highly heterogeneous behavior on spatial and temporal scales. One of the peculiar impacts of varying mixing states was reported on the modification of radiative effects of sulfate and nitrate aerosols in the presence of BC. Global chemistry models have estimated that the net radiative impacts over a region are regulated by relative amounts of BC and sulfate (Ramana et al., 2010). Sulfate aerosols strongly reflect solar radiation while BC strongly absorbs it. However, the net radiative impact of BC is considered to be well amplified in the case of its internal mixing with sulfate (Moffet and Kimberly, 2009). These heterogeneities in aerosol types, mass loadings, composition, and transport make it extremely

complicated for determining future projections of climatic impacts.

The direct effects of aerosols on climate refer to their interference with incoming solar radiation, either through scattering (cooling) or absorbance (warming). The response of aerosols to incoming solar insolation greatly depends on their composition and size. The brighter aerosols (SO_4^{2-}) scatter the solar radiation while the darker aerosols (BC, Brown Carbon) tend to absorb it. The direct effects of aerosols play significant roles in modifying Earth's radiation balance. The properties of aerosols in modifying Earth's radiative budget through changes in cloud microphysical properties come under indirect climatic effects. The vital consequences of aerosol indirect effects are based on the fact that even 5% enhancements in shortwave cloud forcing can recompense the increase in greenhouse gases from 1750 (Ramaswamy et al., 2001). The foremost climatic implications of indirect effects of aerosols result in suppressed precipitation with increased cloud lifetime and the amount of clouds (Albrecht, 1989). Further, an increase in cloud coverage leads to an enhanced albedo (Twomey, 1959), which in turn amends the Earth's radiation budget. With recent advancements in both in situ and satellite-based measurements, significant progress in recognizing the cloud-aerosol interaction has been made. However, quantification of the indirect effect still pose uncertainties in comparison to the direct effects (Schwartz and Andreae, 1996). With enhanced concentrations of anthropogenic aerosols, the evidence of reduced planetary albedo over clouds has been inferred from satellite observations, mostly in regions with high absorbing aerosols (Krüger and Graßl, 2004). A reduction in the albedo of light-absorbing species is recognized as a semidirect effect (Hansen et al., 1997). These collective impacts of aerosols, including direct, indirect, and semidirect effects, on the climate could have major socioeconomic concerns and pose serious threats to the sustainability of the planet (Banerjee et al., 2017a).

3 SATELLITE OBSERVATIONS FOR AEROSOL MONITORING: DEVELOPMENTS

Remote sensing has long been utilized for monitoring airborne particulates using various observational platforms. A complete historical background on the development of aerosol observations through remote sensing is available from Lee et al. (2009) and Kokhanovsky and de Leeuw (2009). However, recent advancements in satellite-retrieved aerosols have been briefly discussed here, especially in terms of polar-orbiting satellites. The polar-orbiting satellites are sun-synchronous satellites that regularly cover the entire globe, providing repetitive coverage on a periodic basis. Due to the large spatial and temporal variability of atmospheric aerosols, remote-sensing products deliver precise information about global distributions of aerosols. The very first of its kind AOD was generated by space-borne spectral measurement using the Multi Spectral Scanner (MSS) onboard the Earth Resources Technology Satellite (ERTS-1) (Griggs, 1975), while the first operational aerosol product was generated in 1978 using the radiometer (Advanced Very High Resolution Radiometer, AVHRR) onboard the TIROS-N satellite. The series of historical satellite sensors still in operation for monitoring Earth's atmosphere and climate are TOMS (Total Ozone Mapping Spectrometer, for ozone) and AVHRR (for weather system). AVHRR, initially launched in 1978, had multiple bands (0.63-11.5 μm) and was used to retrieve AOD and AE. It was subsequently improved and relaunched with NOAA-6∼16. The satellite Nimbus-7 was launched in 1978 having a Stratospheric Aerosol Measurement instrument (SAM-2) which functionally initiated retrieval of aerosol properties on a regular basis. TOMS was also launched in 1978 (with Nimbus-7) and in 1996 (with Earth Probe), it was associated with the measurements of the Absorbing Aerosol Index.

Initially, due to lack of scientific understanding on climatic implications of aerosols, limited efforts were made to retrieve aerosol optical properties from space. All satellite exploration during the initial stages of development in the 1990s was especially focused on retrieving trace gases (like GOME, Global Ozone Monitoring Experiment; SCIAMACHY, Scanning Imaging Absorption SpectroMeter for Atmospheric CHartographY) or land/sea surface temperature and reflectance (SeaWiFS, Sea-viewing Wide Field-of-view Sensor; MERIS, MEdium Resolution Imaging Spectrometer). GOME launched with the ERS-2 satellite in 1995, associated with ATSR-2 (Along-track Scanning Radiometer), which helped to retrieve the first operational and reliable aerosol properties from space. The sensor POLDER (with ADEOS) launched in 1996 was a promising instrument due to its capability for multiple-view measurements for a varied band with spectral polarization for reflected radiation. The finest version of POLDER (POLDER-3) was launched with Parasol in 2002 to measure the polarization of reflected light for identifying airborne fine particulates. It remained functional until 2013. This was subsequently followed by the launch of the Moderate Resolution Imaging Spectro-Radiometer (MODIS) onboard Terra (1999, with Multi-angle Imaging Spectro-Radiometer) and Aqua (2002), AATSR (with ENVISAT, 2002), and OMI (with Aura, 2004), providing multidimensional information on aerosol optical properties. The aerosol retrieval algorithms were further developed for application-based retrieval and to collocate both with ground-based observations. One of the significant inclusions for satellite-based retrieval of aerosol optical properties is CALIOP. It is a typical space-borne LIDAR onboard collocate CALIPSO satellite, which was launched in 2006. The CALIOP has two-wavelength (visible and IR band) polarization-sensitive LIDAR and passive imagers for retrieving the vertical distribution of both aerosols and clouds from the surface to 40 km. Another LIDAR-based sensor, the Geosciences laser altimeter system (GLAS), onboard ICESat was launched in 2003 to determine the elevation and position of each point measurement on the Earth and to identify cloud and aerosols. Most recently, the Visible Infrared Imaging Radiometer Suite (VIIRS) onboard the NPP-Suomi satellite was launched in 2011. It is a successor to MODIS and MISR in terms of retrieving aerosol optical properties from space-borne platforms.

4 SATELLITE RETRIEVAL OF AEROSOL PROPERTIES

4.1 Aerosol Retrieval Algorithms

With consequent development in sensor technology, satellites are frequently being used to obtain information on various products, both on global and regional scales. The information retrieved by satellites depends on the radiation retrieved by the sensor at the top of the atmosphere (TOA), mounted on the satellite on a specific orbit. Satellite-retrieved information may have varying attributes. In terms of information, the optical data may be useful for identifying spatiotemporal variations as well as classifying columnar properties and resolute vertical distributions. Retrieval of aerosol properties from remote-sensing satellites depends on the interaction of tiny airborne particulates with radiation. Upon interaction with particles, radiation is distributed in multiple directions, typically based on particle morphology and chemical composition. Aerosol retrieval algorithms use angular distributions of radiation scattering after proper isolation of various atmospheric and surface interferences.

The retrieval process fundamentally poses three constraints: cloud effects, surface reflectance, and molecular scattering. In principle, the retrieval of aerosol properties depends on the reflected radiation. However, in the presence

of clouds, such reflection is dominated by the clouds themselves over aerosols. Any cloud effects may thereby reduce the possibility of retrieving minute variations in aerosols while excessive cloud screening may remove areas with higher aerosol loading. Thus, often cloud screening is the first and most important step in any aerosol-retrieval algorithm (Lee et al., 2009). Cloud screening may be achieved by various means such as identifying wavelength dependence in the visible to the thermal infrared (IR), spatiotemporal analysis, using the O_2 A-band ,or by using multiple concurrent observations (Ackerman et al., 1998). Contribution of land surface reflectance radiation to the TOA is the second important constraint in remote sensing that needs to be isolated based on recognizing land surface properties varying from a dark surface (ocean, forest) to brighter ones (bare soil, urban habitat, industrial area, permafrost). Considering variations in surface reflectance, it is essential to set a boundary upon which atmospheric contributions are measured (Kokhanovsky and de Leeuw, 2009). On this account, retrieval of aerosol properties over oceans is relatively easy and straightforward; upon land, however, multiple corrections need to be made to remove interference. The third significant step in satellite retrieval is to account for path radiance, which considers both molecular scattering and absorption by various atmospheric molecules and gases. A Radiative Transfer Model (RTM) is generally applied to account for path radiance for a specific sun-satellite geometry.

An aerosol-retrieval algorithm uses the radiance measured at the TOA and compares it to that calculated by the RTM over a range of aerosol models for recognizing the best model to retrieve aerosol properties. Radiative transfer calculations are made for a variety of discrete situations, including a set of wavelengths that are used in retrieval, viewing geometries (viewing and solar zenith angle, relative azimuth angle), surface pressure, and AOD ranges (Kokhanovsky and de Leeuw, 2009). The calculations are time-consuming; therefore they are made outside the actual algorithm and then stored in look-up tables (LUTs). Each aerosol model has its own LUTs and contains multiple parameters such as path reflectance (R_a); total transmittance from the TOA to surface (T_a) and surface to satellite (T_b); the spherical albedo (r); AOD (τ); aerosol phase functions ($P(\theta)$); scattering angle (θ); and single-scattering albedo (ω). The TOA reflectance (R), ratio of radiance received by sensor over that reaching to the TOA (E_0) may be represented as:

$$R = \frac{\pi I}{E_0 \mu_0} \tag{1}$$

where, I is the intensity of reflected light and μ_0 is the cosine of the observation angle. The TOA reflectance with albedo A and wavelength λ is presented as:

$$R = R_a + \frac{A T_a T_b}{1 - A_r} \tag{2}$$

Now, except surface albedo, all the other parameters depend on AOD (τ) which is, in fact, the integral of the extinction of light ($K^a_{ext} z, \lambda$; aerosol extinction coefficient at height z for wavelength λ) caused by airborne particulates over a vertical column (height of TOA, H) through the atmosphere. Therefore, AOD may be computed as:

$$\tau(\lambda) = \int_0^H K^a_{ext}(z, \lambda) dz \tag{3}$$

The spectral dependence of AOD from satellite measurements of spectral reflectance (R) requires precise isolation. The surface albedo needs to be retrieved or rejected using multiview observations (Kokhanovsky and de Leeuw, 2009). For most atmospheric conditions, the value of A_r remain <0.1, and therefore, for the dark land surfaces ($A \to 0$) the product A_r may be ignored. The choice of appropriate LUTs for path reflectance, spherical albedo, and for T_a and T_b either must be assumed or considered based on the region of interest. The LUTs are

typically made by the vector radiation transfer equation for collection of aerosol models representing a specific area (Levy et al., 2007). The algorithm selects the LUT for the appropriate aerosol model that best fits the observed spectral reflectance by the satellite sensor. However, such consideration also depends on the climatology (Levy et al., 2007) derived from observations (Levy et al., 2007) or the transport model for a particular area (Curier et al., 2008).

4.2 Aerosol Optical Properties

The optical properties of aerosols are important for atmospheric visibility and climate-related studies. Advancements in satellite remote sensing have made it possible to retrieve several aerosol optical properties from space with global coverage. These remote-sensing techniques include both passive and active sensors. Some of the important optical properties of aerosols include AOD, the Angstrom exponent (α), the turbidity coefficient (β), the single-scattering albedo (SSA), the refractive index, the absorption and extinction coefficients, the phase function $P(\theta)$, the asymmetry parameter (g), the phase matrix, and the backscatter properties.

(i) Aerosol optical depth

AOD is defined as the integral of the extinction coefficient over a vertical column of atmosphere of the unit cross-section. The extinction coefficient refers to the depletion of radiance per unit path length (also termed attenuation). AOD depicts the extinction of solar radiation by aerosols in open atmosphere. Typically, aerosols—based on their morphology and chemical composition—attenuate the solar radiation either by absorbing or scattering. It is a dimensionless entity and it relates the amount of aerosols in the vertical column of atmosphere. A typical value of AOD as 0.01 represents an extremely clean environment while AOD values above 0.5 correspond to a hazy atmosphere, which may be extended to 5.0 at certain cases. The measurement of total optical depth is based on the Beer-Lambert-Bouguer law considering the following equation:

$$V(\lambda) = V_o(\lambda) d^2 \exp\left[-\tau(\lambda)_{TOT} * m\right] \tag{4}$$

where V is the digital voltage measured at wavelength λ; V_o is the extraterrestrial voltage; d is the ratio of the average to the actual Earth-Sun distance; τ_{TOT} is the total optical depth; and m is the optical air mass (Holben et al., 1998). The optical depth (τ) for wavelength λ with α as the extinction coefficient of the atmosphere having the path z as an inconvenient unit, can be defined as:

$$\tau_\lambda = \int_z^\infty \alpha(\lambda, z')dz' \tag{5}$$

At surface ($z=0$), the τ will be τ^* by definition while at the TOA, $\tau=0$. Since radiation is subject to attenuation due to other wavelength-dependent trace gases, water vapor, and Rayleigh scattering, AOD can be obtained after subtracting the optical depths from all other components from the total optical depth.

So, the equation for computing AOD turns to:

$$\begin{aligned}\tau(\lambda)_{\text{Aerosol}} = \tau(\lambda)_{TOT} - \tau(\lambda)_{\text{water vapor}} - \tau(\lambda)_{\text{Rayleigh}} \\ - \tau(\lambda)O_3 - \tau(\lambda)NO_2 - \tau(\lambda)CO_2 \\ - \tau(\lambda)CH_4\end{aligned} \tag{6}$$

where $\tau(\lambda)$ is the respective optical depths from different atmospheric components.

The primary applications of AOD in atmospheric and environmental sciences include atmospheric correction of remotely sensed surface features, monitoring of sources and sinks of aerosols, monitoring volcanic eruptions and forest fires, monitoring air quality, health and epidemiological studies, climate change studies, and radiative transfer studies.

(ii) Angstrom exponent (α)
The Angstrom exponent (α) is an optical property of aerosols that provides the information on aerosol size distribution. The Angstrom exponent is estimated from AOD, typically from 440 to 870 nm. It is the negative slope of AOD for a particular wavelength in logarithmic scale. It can be calculated from two or more wavelengths (like λ and λ_0) using a least squares fit.

$$\tau = \tau_{\lambda_0}\left(\frac{\lambda}{\lambda_0}\right)^{-\alpha} \tag{7}$$

$$\alpha = \frac{\ln {}^{\tau_1}/_{\tau_2}}{\ln {}^{\lambda_2}/_{\lambda_1}} \tag{8}$$

where α is the Angstrom exponent; τ is the AOD; and λ is the wavelength. The values of a above 2.0 designate finer aerosols such as smoke and sulfates whereas values close to zero specify the presence of coarser particles such as desert dust.

(iii) Turbidity coefficient (β)
Turbidity coefficient (β) is a dimensionless quantity that measures the opacity of a vertical column of atmosphere (Utrillas et al., 2000). The Angstrom turbidity coefficient indicates the total aerosol content of the atmosphere in the zenith direction. It can be defined as the aerosol optical thickness corresponding to a wavelength of 1 μm. Since the Angstrom formula is just an approximation, it may not be valid over an extensive spectral range. However, the Angstrom formula seems to provide a good parameterization of spectral AOD between 400 and 670 nm bands (Martinez-Lozano et al., 1998). The Angstrom turbidity coefficient can be calculated as:

$$\beta = \tau \cdot \lambda^{\alpha} \tag{9}$$

where β is the turbidity coefficient; τ is the AOD; λ is the wavelength in micrometers; and α is the wavelength exponent representing the aerosol size distribution (Angstrom, 1964). Turbidity coefficients <0.1 are associated with a relatively clear atmosphere while values >0.2 are associated with a relatively polluted atmosphere.

(iv) Asymmetry parameter and phase function
The asymmetry parameter (g) represents the degree of asymmetry of the angular scattering and is a measure of the preferred scattering direction (forward or backward) for the light coming across the aerosols. It is equal to the mean value of μ (the cosine of the scattering angle), weighted by the angular scattering phase function $P(\mu)$. The asymmetry parameter corresponding to +1 represents the scattering strongly peaked in the forward direction (scattering by larger particles) whereas −1 denotes entirely backscattered light. Asymmetry parameters equal to 0 represent an evenly distributed scattering mostly from smaller particles (Rayleigh scattering). Asymmetry parameter may be defined as:

$$g = {}^{1}/_{2}\int_{-1}^{1} d(\cos\theta)p(\theta)\cos\theta \tag{10}$$

where θ is the angle between incident light and scattering direction and $P(\theta)$ is the angular distribution of scattered light (the phase function). The asymmetry parameter strongly depends on the particulate size. Phase function is defined as the energy scattered per unit solid angle in a given direction to the average energy in all directions. Phase functions may be expressed as:

$$p(\theta) = \frac{4\pi}{C_{sca}}\frac{dC_{sca}}{d\Omega} \tag{11}$$

$$C_{sca} = \int_{4\pi} d\Omega \frac{dC_{sca}}{d\Omega} \tag{12}$$

where $dC_{sca}/d\Omega$ is the differential cross-section and C_{sca} is total scattering cross-section.

(v) Single-scattering albedo (ω)
A single-scattering albedo (SSA) is the measure of effectiveness of light scattering due to atmospheric aerosols relative to its total extinction. It can be defined as the ratio of scattering and extinction coefficients (scattering + absorption) at a given wavelength. SSA is a dimensionless entity with values ranging from 0 (dominance of absorbing aerosols) to 1 (light extinction mostly due to scattering aerosols). It is an important optical parameter for aerosol radiative transfer studies for its use in the calculation of scattering phase function and as an input to the OPAC model for the calculation of aerosol radiative forcing. Not limited to this, SSA can be used to characterize the type of aerosols. Eq. (13) describes the mathematical expression for SSA:

$$\omega = \frac{\sigma_s}{\sigma_s + \sigma_\alpha} \tag{13}$$

where σ_s and σ_a are the aerosol scattering and absorption coefficients, respectively.

(vi) Mass extinction coefficient (B_{ext})
The mass extinction coefficient (B_{ext}) of aerosol represents how strongly particulates absorb/scatter radiation at a given wavelength per unit mass in a constant volume. The mass extinction coefficient depicts the area of extinction for a unit mass of the aerosol (usually in units of (m^2/g)). Mathematically, it can be expressed as:

$$B_{ext} = \frac{3QM}{4\rho rMd} \tag{14}$$

where B_{ext} is the aerosol mass extinction efficiency; Q is the extinction coefficient; M is the total aerosol mass loading (dry mass + mass of water taken by the aerosols); ρ is the particle density; r is the particle effective radius; and Md is the dry aerosol mass (Chin et al., 2002).

5 SATELLITE AEROSOL DATABASE

Recent advancements in space sciences and remote-sensing technologies have endowed enormous prospects for studying aerosol and other atmospheric properties using satellite-based measurements. Though these techniques deliver a diverse range of information, retrieving them for applications is complicated and requires specific skills, tools, and computation facilities. Additionally, due to extremely large datasets, variation in data types, metadata, and the availability of various platforms for data access make the selection criteria even more critical. Several web tools and Internet-based resources are now available that offer ready-to-use aerosol products to end users with different resolutions, data types, and applications. These tools provide information on global aerosol distribution and properties in the form of imagery, maps, and easily executable files that can be processed further for different air-quality applications.

The web tools for aerosol-related information offer direct access to available satellite data products of various resolutions (raw or fully processed), time series, data analysis, software, and programming tools. The satellite products available from NASA are managed through NASA's Earth Observing System Data and Information System (EOSDIS). This not only provides data to the end users but also allows spatial subsetting to large global data files. Various other platforms including the Goddard Earth Sciences Data and Information Services Center (GES DISC) and the Langley Research Center Atmospheric Science Data Center (LaRC ASDC) provide information about different gaseous and aerosol products. Some specific web tools for exceptional events like fire information and hazard mapping are also available. These are being used in collocation with the information available through other tools. Also, clubbing spatially resolved data with GIS has

made data analysis relatively easy. Other options for graphical representation of data are also available through selected searches and selection of required parameters on spatial and temporal scales. NASA's Fire Information for Resource Management System (FIRMS) provides fire-related information in the form of shaped files of predefined grids, which helps in accessing, analyzing, and forecasting fire events on a long-term basis. Some other popular tools available are LAADS Web, Worldview and Giovanni. Table 1 presents different web-based tools and resources for retrieving, analyzing and applying satellite-retrieved aerosol data products that are most commonly used by the scientific communities.

In recent years the diverse applications of multipurpose satellite data by several agencies have led to the development of common platforms for data access and use. NASA, NOAA, and EPA have initiated a partnership for the assessment, management, and prediction of air quality by infusing various satellite measurements for public benefit. All relevant information has been provided on a common platform known as IDEA (Infusing satellite Data into Environmental air quality Applications). Along with resources for data availability, there are some specific web tools (like ARSET) that provide online training for the application of satellite retrieval for aerosols and other air quality parameters.

5.1 Retrieval of Aerosol Properties From MODIS

The Moderate Resolution Spectroradiometer (MODIS) sensor flew onboard the sun-synchronous, near-polar satellites Terra and Aqua from 1999 and 2002, respectively. The MODIS instrument observed the earth from a 700-km altitude (±55 degrees view scan) with a swath of about 2330 km. This means it had nearly global coverage every 1–2 days on a daily basis with 16 days of repeat cycle (http://modis.gsfc.nasa.gov). The different orbital paths of MODIS-Terra and MODIS-Aqua gives different overpass times at morning (Terra descending node 10.30 local time) and afternoon (Aqua ascending node 13.30 local time) over the equator, which allows MODIS to observe the earth two times during the day. MODIS instruments measured in the 36-wavelength band (0.4–14.4 μm), with ground spatial resolution at nadir 0.25×0.25 km (bands 1–2), 0.5×0.5 km (bands 3–7), and 1×1 km (bands 8–36). The data retrieved by MODIS is organized into 5-minute sections called granules. It is designed to be spectrally stable (better than 2 nm) and adequately sensitive related to aerosol properties with absolute radiance calibrated to within 2% (Guenther et al., 2002). Originally intended for climatic applications, it has wide applicability in air quality, especially in terms of aerosol columnar optical depth and size distributions (Fig. 3A and B).

MODIS uses three separate algorithms for retrieving aerosol optical properties over land and oceans: the Dark Target (DT) algorithm over land (Kaufman et al., 1997; Levy et al., 2007), the DT algorithm over ocean (Tanré et al., 1997), and the Deep Blue (DB) algorithm over land (Hsu et al., 2004). The DT algorithm is used to retrieve aerosol optical properties over oceans and dark land (vegetated area). It is based on the concept that in the visible band within an atmospheric *window*, aerosol tends to brighten while vegetation appears dark (Kaufman et al., 1997). Such spectral contrast is purposefully used for retrieving aerosol properties. It was originally developed by Kaufman et al. (1997) over land and by Tanré et al. (1997) over ocean. The principal products for DT algorithms include the total AOD (τ) at 0.55 μm with an estimate of fine-mode fractions (FMF, η) to the total optical depth. However, there are some basic constraints in using the DT algorithm by single-view sensors (SeaWiFS, VIIRS, AVHRR, and

TABLE 1 Satellite Data Access, Visualization, and Analysis Web Resources for the End User

Database Type	Agency	Database/Resource	Website
Online training and webinars	NASA	Applied remote sensing training	http://arset.gsfc.nasa.gov/
Data, tools, and modeling	NASA	Air Quality Applied Sciences Team	http://acmg.seas.harvard.edu/aqast/
Search, access, and downloading files, with options for subsetting	NASA	Reverb	http://reverb.echo.nasa.gov/reverb
Visualization and downloading data	NASA	Land Atmosphere Near-real-time Capability for EOS	https://earthdata.nasa.gov/data/near-real-time-data/
Data and imagery	NASA	Goddard Earth Sciences Data and Information Services Center	http://disc.sci.gsfc.nasa.gov
Web-based interactive visualization and analysis	NASA	Giovanni	http://disc.sci.gsfc.nasa.gov/giovanni/
Worldview		An interactive visualization and analysis web tool	https://earthdata.nasa.gov/labs/worldview/
Data and imagery	NASA	Mirador	http://mirador.gsfc.nasa.gov
Data and imagery	NASA	Langley Research Center Atmospheric Science Data Center	http://eosweb.larc.nasa.gov
MODIS and VIIRS data and imagery	NASA	Level 1 and Atmosphere Archive and Distribution System	http://ladsweb.nascom.nasa.gov
True color imagery and smoke	NOAA	Hazard Mapping System Fire and Smoke Product	http://www.ospo.noaa.gov/Products/land/hms.html
data and imagery for fire locations	NASA	Fire Information for Resource Management System	http://earthdata.nasa.gov/data/near-real-time-data/firms
Data visualization	NOAA-NASA-EPA	Infusing Satellite Data into Environmental Applications	http://www.star.nesdis.noaa.gov/smcd/spb/aq/
Software package		International MODIS/AIRS Processing Package	http://cimss.ssec.wisc.edu/imapp/ideai_v1.0.shtml
Data and modeling	EPA	Remote Sensing Information Gateway	http://ofmpub.epa.gov/rsig/rsigserver?index.html
Data Analysis	EPA	Exceptional Event Decision Support System	http://www.datafed.net
Data Acquisition	ESA	Earth Online	https://earth.esa.int/web/guest/data-access
Browse and download imagery of EOS satellites	NASA	NASA Earth Observations	http://neo.sci.gsfc.nasa.gov/

Modified from Duncan, B.N., Prados, A.I., Lamsal, L.N., 2014. Satellite data of atmospheric pollution for U.S. air quality applications: examples of applications, summary of data end-user resources, answers to FAQs, and common mistakes to avoid. Atmos. Environ. 94, 647–662.

MODIS) over desert and semidesert regions. In particular, TOA reflectances received by satellite sensors at 620–850 nm (red to far red) are usually overshadowed by surface reflectance, especifically over a bright land mass (desert area). Further, AOD retrieved on the mid-visible wavelength is mostly low around the world (Hsu et al., 2004). This leads to aerosol retrievals by single-view sensors (SeaWiFS, VIIRS, AVHRR, and MODIS) using the DT algorithm being practically unsuitable for scientific exploration.

The DB algorithm was originally developed for retrieving aerosol optical properties over bright reflecting surfaces to fill the gaps in the DT algorithm, which was especially designed to retrieve aerosols over dark surfaces (Hsu et al., 2004; Levy et al., 2007). The DB algorithm used the blue channels (412 and 470 nm) whereas the surface reflectance at shorter wavelength channels is much lower than the longer wavelength channels (Hsu et al., 2004). The DB algorithm retrieves aerosol for cloud-free and snow/ice-free pixels at nominal spatial resolution 1×1 km and before aggregate to 10 km. In contrast, the DT algorithm aggregates pixels at nominal 500 m–10 km (20×20 pixels) and 3 km resolution (6×6 pixels), and retrieves aerosol after screening for cloud and snow/ice (Levy et al., 2013). The latest update of the aerosol MODIS retrieval algorithms over land and oceans known as collection 6 (C6) for all three algorithms over land and ocean (Levy et al., 2013; Sayer et al., 2013; Hsu et al., 2013). DT algorithms over land and oceans were updated several times, with the major update known as C5. This is considered the second generation of DT algorithms (Levy et al., 2007; Remer et al., 2008). However, the DT algorithms were updated without change in the principle of the C5. The major changes include quality assurance (QA) assignment, the assumption of Rayleigh optical depth and gases, and updating the cloud mask that allows the detection of thin cirrus cloud over oceans (DT-ocean) and retrieving heavy smoke over land (DT-land). In addition to refinement and improvement of aerosol retrieval over land and ocean, DT C6 algorithms also include aerosol data products at 3 km resolution in addition to the standard aerosol data products at 10 km. The 3 km products have the advantage in retrieving aerosols over a small scale, which allows local variability in aerosols (Kumar et al., 2015b, 2017). The first generation of the DB algorithm known as C5 was developed to retrieve aerosols over only bright surfaces. The second generation of the DB algorithm known as C6 was extended to retrieve aerosols over the entire land mass (except snow/ice surfaces), not only over bright surfaces. The improvement in surface reflectance determination, cloud screening, and updated aerosol model schemes allows the algorithm to increase the spatial retrieval coverage to vegetated surfaces (Hsu et al., 2013). In order to fill the gaps and improve visualizations of DT and DB algorithms over land, C6 includes a new dataset (Dark_Target_Deep_Blue_Optical_ Depth_550_-Combined) based on merged DT and BD products at a standard resolution of 10 km. The data merged based on the NDVI pixel value at spatial resolution 0.25 degrees for each month. For the pixel that has $\mathrm{NDVI} \leq 0.2$, DB data are used. For the pixel having $\mathrm{NDVI} \geq 0.3$, DT data are used. For the transition region ($0.2 \leq \mathrm{NDVI} \leq 0.3$), the data that has the higher QA flag are used, and if both have $\mathrm{QA} = 3$ the mean value of DT and DB data are considered (Levy et al., 2013).

The MODIS algorithm products have been evaluated and compared with ground-measured AERONET aerosol data on a global scale. Remer et al. (2013) evaluated DT 3 km AOD and reported it to be 0.01–0.02 higher than 10-km AOD over land while retrieving a proportionally higher number of very low AODs over ocean. The expected error (EE) of the DT algorithm over land at 3 km resolution is $\pm(0.05 + 0.20$ AOD) and $\pm(0.05 + 0.15$ AOD) at 10 km resolution (Levy et al., 2013; Remer et al., 2013). The EE of DT algorithm at 10 and 3 km

resolution over ocean is ±(0.03 + 0.05 AOD) (Levy et al., 2013; Remer et al., 2013). Sayer et al. (2013) evaluated the highest quality (QA = 3) DB AOD against AERONET at a global scale and reported the EE of DB AOD is ±(0.03 + 0.15 AOD). Further, Sayer et al. (2014) compared Aqua's second generation DB, DT, and merged dataset with respect to AERONET and concluded that neither algorithm consistently outperformed the other and, in many cases, all the algorithms are equally suitable for quantitative applications.

Multispectral sensing over a wide range of wavelengths has made MODIS a popular sensor among researchers with its extensive applications, such as in air quality studies (Kumar et al., 2017a), long-term climatology (Gupta et al., 2013), meteorological applications (Yu et al., 2013), and studying extreme events (Youn et al., 2011; Kumar et al., 2016, 2017b). Based on the interaction of the majority of aerosols in the visible range of solar spectra, MODIS aerosol products have been widely used at 550 nm. Initial applications of MODIS data collections for aerosol-related studies include distribution of aerosol load, size distribution, and radiative impacts on various spatial and temporal scales. Gupta et al. (2013) using MODIS collection 5 Level 2 observations reported around 80% of days have unhealthy air quality in Lahore. The alarming levels of pollution leading to unhealthy conditions greatly depend on the seasonality of aerosol loadings over any region. Based on 5 years of observations of MODIS AOD and the Angstrom exponent, Che et al. (2013) noted a clear enhancement of aerosol load during spring and summer over the Taklimakan desert in China due to dust events.

Over the Indo-Gangetic Plain, the highest aerosol loadings have been reported during winter due to improved source strength and stable meteorological conditions (Kumar et al., 2015b; Murari et al., 2015; Sen et al., 2014, 2017). Fig. 4 represents the 5-years variations (2011–15) of MODIS AOD and FMF over the entire Indian subcontinent, which clearly identifies the spatial pattern of aerosol loading. Sen et al. (2017) compared AOD both over the IGP and the Indo-Himalayan Plain (IHP) during the winter and summer monsoons of 2014–2015 at multiple locations and concluded a continental outflow from the IGP to the Bay of Bengal. Recent advancements in space technology have opened up its utility in multidisciplinary research, including the estimation of

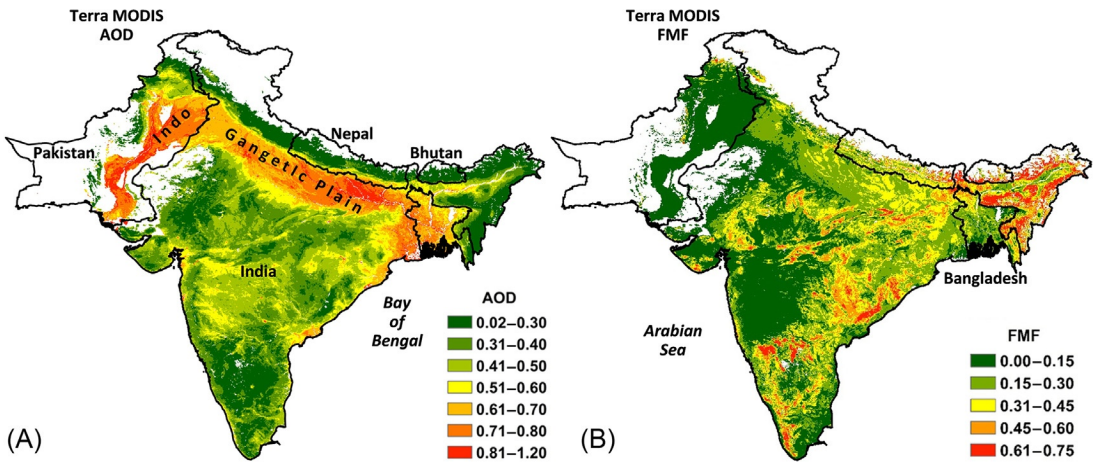

FIG. 4 Comparative figure of Terra MODIS (A) mean AOD (B) mean fine-mode fractions over South Asia for 2011–15.

population exposure to air pollution and mortality assessments based on satellite retrievals. Hu (2009), using collection-5 MODIS AOD data and its collation with near surface $PM_{2.5}$, reported an increase in cancer-induced mortality with an increase in $PM_{2.5}$ concentrations over the United States. The global estimates of mortality attributed to $PM_{2.5}$ concentrations based on MODIS were found comparable to the chemical transport model simulations for anthropogenic $PM_{2.5}$ (Evans et al., 2013). MODIS-based retrievals of aerosol properties have also been used for crop modeling, vegetation, and other climatological studies.

5.2 Aerosol Properties From MISR

The basic complication for a single-view satellite sensor (like MODIS) is the requirement for absolute reflectance or its spectral deviation at multiple wavelengths (Hsu et al., 2006). However, flexibility increases for the multiview satellite sensors (like MISR), which can scan a particular scene with multiple viewing angles and thereby reduce assumptions about surface reflectance. MISR is one of five sensors onboard the Terra satellite, which observes the earth from a polar orbit approximately 700 km above the surface. The sensor has nine cameras, each one fixed at a particular viewing zenith angle in a long-track direction with four spectral bands (446, 558, 672, and 866 nm). The cameras are arranged in different view angles, one at nadir and the other symmetrical views at 26.1 degrees, 45.6 degrees, 60.6 degrees, and 70.5 degrees aft. Each camera in the MISR sensor measures the reflected radiance in four different spectral bands (446, 558, 672, and 866 nm) in a cross-track with spatial resolution varying from 250 m (nadir) to 275 m (off-nadir). MISR has a global coverage of nine days with repeat coverage between 2 and 9 days based on the latitude. The sensor takes measurements in two modes: local and global. In the local mode, which is more of a specific type, each of the nine cameras obtains images at the four spectral bands (i.e., 36 channels) at a spatial resolution of 250–275 m, having a swath width varying from 378 (nadir) to 413 km (off-nadir). In the global mode, the nadir camera retrieves an image in four spectral bands at a spatial resolution of 250 m while the other eight cameras obtain images only by the red band with 250–275 m resolution. MISR products are further radiometrically calibrated, geolocated, and averaged to uniform resolution of 1.1 km (Level 1B2) and are available over both land and ocean at 17.6×17.6 km resolution with 16×16 homogenous arrays.

The aerosol retrieval algorithm of MISR takes advantages of the aerosol composition and relates its physicochemical and optical properties more fundamentally with the TOA radiance received by the sensor. It provides a generic representation in terms of SSA, aerosol size, and phase functions. This allows the user to directly interpret information about aerosol sources and enables comparison with various aerosol types over a region (Fig. 5). The MISR aerosol algorithm retrieves AOD and aerosol type by analyzing MISR TOA radiances from 16×16 pixel patches of 1.1-km resolution. To improve the retrieval algorithm, a series of theoretical experiments were carried out before its launch to determine the acceptability of the retrieval process under varying AODs and microphysical properties (Kahn et al., 2001). The aerosol retrieval process has three basic ancillary datasets: (1) the Terrestrial Atmosphere and Surface Climatology (TASC) dataset for climatological, meteorological, and ozone; (2) Aerosol Climatology Product (ACP) consisting of the aerosol physical and optical properties (APOP) file and a tropospheric aerosol mixture file having information on aerosol microphysical and scattering characteristics of 21 different aerosol compositions; and (3) a Simulated MISR Ancillary Radiative Transfer (SMART) dataset for large dark water bodies (for oceans) and spectrally black surfaces (for land). The fundamental process in aerosol retrieval involves comparing MISR-observed TOA radiances with modeled

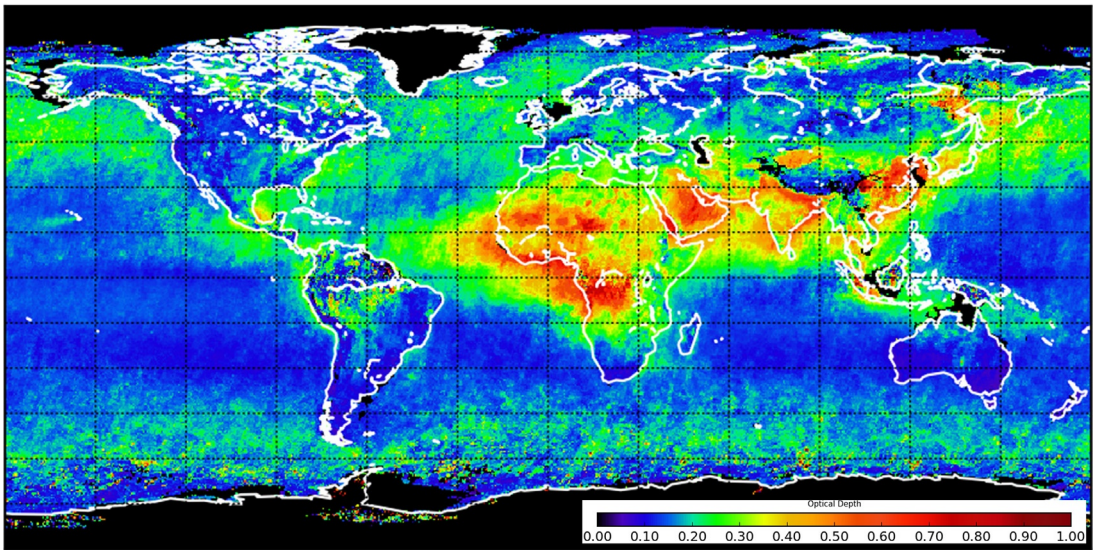

FIG. 5 Global mean (2011–2015) aerosol optical depth retrieved from MISR.

reflectance derived from a coupled atmosphere/surface RTM. The MISR RTM is defined by its base, top and scale heights, and optical depth. The RT calculations are performed using a scalar code based on a matrix operator technique including a correction for Rayleigh polarization effects. Further, within the SMART database containing multiple RT parameters (function of AOD, aerosol component, and view angles), RT calculations are carried out for individual aerosol components required to retrieve aerosols. The MISR under generic retrievals has the capability of distinguishing aerosols in 3–5 size groups and 2–4 compositional groups (by means of SSA; Kahn et al., 1998). It can also distinguish between spherical and nonspherical particulates (Kahn et al., 1997). Under climatological retrievals, MISR has the capability of identifying sea salt, BC, and dust within 20% or more of each component's AOD fraction. Kahn and Gaitley (2015) evaluated the MISR Version 22 aerosol-type self consistency in comparison to the Aerosol Robotic Network aerosol-type climatology and reported aerosol-type differentiation decreases below 0.15 or 0.20 AOD.

Kahn et al. (2010) assessed the quality of MISR version 22 (V22) aerosol products over land and oceans, comparing the MISR data with coincident observations from 81 globally distributed AERONET sites for 8 years. The study reported that most of the MISR AOD retrievals fall within 20% of AOD of the paired validation data, and about 50%–55% are within 10% × AERONET AOD, except sites where dust and smoke dominate. Most of the validation studies reported that MISR has greater accuracy in retrieving aerosol optical properties. Other studies also compared MISR-MODIS AOD against AERONET AOD and revealed that the MISR-AERONET comparison shows strong correlation compared to the MODIS-AERONET. Bibi et al. (2015) observed a higher degree of association with AERONET over oceans in comparison to land whereas Qi et al. (2013) reported better performance of MISR data over selected sites compared to MODIS. Additionally, MISR aerosol products have been utilized for the assessment of long-term global trends of aerosol distribution. Mehta et al. (2016) reported increasing trends in AOD over Asian and

African land masses and surrounding regions while declining aerosol trends were reported over Europe, South America, and North America. A better predictability of near-surface $PM_{2.5}$ was observed by You et al. (2015) using MISR AOD (72%) over MODIS AOD (67%), opening up an improved scope for estimating ground-level particulates using MISR aerosol retrievals. In a unique approach to link MISR-derived AOD with BC aerosols, Zeeshan and Oanh (2015) reported a high capacity of MISR AOD in estimating daily BC in Bangkok, Thailand.

5.3 Aerosol Properties From AATSR

The Advanced Along-Track Scanning Radiometer (AATSR) is a remote-sensing instrument onboard the satellite ENVISAT (ENVIronmental SATellite) of the European Space Agency (ESA). The mission is the continuation of ATSR-1 and ATSR-2 on the European Remote Sensing (ERS) satellite. It has been enlisted as part of a series of advanced instruments designed primarily for the measurement of sea surface temperature (SST), while products like AOD (at 555, 659, 865, and 1610 nm) and AE are also explored. With a data resolution of 1 km at the nadir, AATSR provides measurements of reflected and emitted radiation for a wide range of wavelengths. The most peculiar feature of AATSR includes the use of a conical scan for a dual view of Earth's surface, onboard calibrations, and mechanical coolers for the maintenance of the infrared detectors. AATSR was launched in March 2002, following the ATSR-2, and was in operation through May 2012. It was primarily launched as a geophysical ocean sensor for the measurement of SST. However, it was also utilized for other land applications. AATSR provided information on SST, clouds, aerosols, vegetation, and snow cover in addition to calibrated reference radiances and imagery. The swath width of AATSR is approximately 512 km wide, assuring average global coverage every five days over the equator with more frequent at higher latitude. Although, AATSR does not provide daily global coverage, it has an extended data product of 20 years of aerosol properties over land. At the nadir, retrieval is made for single pixels (1×1 km) and subsequently groups of 10×10 pixels are averaged to reduce noise and errors.

Two different aerosol retrieval algorithms have been developed for AATSR, the first using the single view over oceans (Veefkind and de Leeuw, 1998) while the other uses the double view over land (Veefkind et al., 1998). The special dual-view algorithm is used for the compensation of land reflectance over land. The dual-view capacity of AATSR over land provides improved cloud screening (de Leeuw et al., 2007). This algorithm has been validated with AERONET data (Robles Gonzales et al., 2000) and also from other aerosol-retrieval instruments such as MISR and MERIS. The retrieval algorithm is based on the construction of an aerosol model with two different aerosol types. The reflectance at the TOA is computed using RTM and further compared with the reflectance measured by the AATSR device. The model that results in the minimum discrepancy between the modeled and measured TOA reflectance was used for the determination of aerosol optical properties. The algorithm used for AATSR aerosol retrieval separates the surface bidirectional reflectance from the atmospheric aerosols without recourse to a priori information of the land surface properties (North et al., 1999). The ratio of surface reflectance at the nadir and forward viewing angles is well correlated between bands. North et al. (1999) further considered the variation of the diffuse fraction of light with wavelength. However, the algorithm is subject to discrepancies in retrieving AODs under cloudy conditions. Over the ocean, the aerosol properties are directly retrieved using single view. The accuracy of the AATSR algorithms was estimated at 0.03 over the ocean and 0.05 over land in comparison to AERONET (de Leeuw et al., 2007).

AATSR observations have varying applications, especially over the regions with varying aerosol compositions like the Indian Ocean (Robles-Gonzalez et al., 2006). The main aerosol products of AATSR are AOD and aerosol types, while the aerosol mixing ratio is also available in principle. Bevan et al. (2012) presented a long-term (2003–2009) global dataset of aerosol properties from the AATSR for a wide variety of surfaces including ocean, vegetated land, and desert. The AATSR datasets were compared with AERONET and the Maritime Aerosol Network (MAN), and with MODIS and MISR aerosol products. Agreement with AERONET ($r=0.80$; $\Delta\tau=\pm0.025\pm0.4\tau$) and MAN ($r=0.97$; $\Delta\tau=\pm0.04$) was reported to be high while monthly AODs from MODIS and MISR represented close agreement over most of the regions. The global mean values of AOD at 550 nm over land and ocean were reported to be 0.195 and 0.137, respectively. Bevan et al. (2009) used 13 years (1995–2004) of AATSR AOD over the Amazon forest to recognize the role of aerosols in biosphere-climate interactions. A decreasing trend in dry-season AOD (1995–2000) and subsequent increase (2000–2004) was explained in terms of deforestation practices over the region.

5.4 Aerosol Properties From CALIOP

The Cloud-Aerosol LIDAR with Orthogonal Polarization (CALIOP) is a space-borne LIDAR onboard the Cloud-Aerosol LIDAR and Infrared Pathfinder Satellite Observation (CALIPSO) satellite. It retrieves the vertical distribution of aerosols and clouds on a global scale (Winker et al., 2009; Kittaka et al., 2011; Kumar et al., 2016). The active laser provides a high vertical resolution aerosol profile in cloud-free conditions as well as above lower-lying clouds and below optically thin clouds. It was developed within NASA's Earth System Science Pathfinder (ESSP) program in collaboration with the French space agency Centre National d'Études Spatiales (CNES) for observing global distribution and properties of aerosols and clouds. CALIPSO was launched in April 2006 with the CloudSat satellite as part of the NASA A-train. It has a 705 km sun-synchronous polar orbit with an equator crossing at 13:30 local time. CALIPSO carries two sensors: (1) an active LIDAR CALIOP; and (2) two passive sensors, the Imaging Infrared Radiometer (IIR) and Wide Field Camera (WFC), which obtain data in the infrared and visible spectral regions, respectively. All the sensors work independently and continuously except the WFC sensor, which only works in daylight. The LIDAR provides high-resolution measurements of aerosol and cloud vertical distribution, which improves understanding about the effect of aerosols and clouds over climate (Winker et al., 2009). It has a swath with practically zero width with a vertical resolution of 30–60 m, having successive footprints spaced by 333 m along the orbit track. It measures the aerosol vertical profile with an elastic laser backscatter at 1064 nm with a parallel and cross-polarized return signal at 532 nm. However, the daytime profile records a slightly lower signal-to-noise ratio over nighttime due to solar background illumination. Within −0.5 to 8.2 km altitude, both the 532 and 1064 nm signals have a horizontal resolution of 330 m and vertical resolution varying from 30 to 60 m, respectively. Above 8.2–20.2 km, both profiles are averaged to 60 m vertical and 1 km horizontal resolution. The *level 0* data are reconstructed, unprocessed with full resolution while reconstructed, geolocated, and altitude-registered Level 1 data are calibrated before being processed for Level 2.

The CALIPSO aerosol-retrieval process is derived on the basis of cluster analysis of a multiyear (1993–2002) AERONET dataset. Six AERONET aerosol clusters were considered based on observed physical and optical properties (Omar et al., 2005). The AERONET-derived parameters were further adjusted to develop a more accurate LIDAR ratio related to actual

observations. Out of six, only three (biomass burning, polluted continental, and polluted dust) were further adopted as CALIPSO aerosol models. Further, marine and background/clean continental aerosol models were developed both by direct measurements of particle size distributions and refractive indices or through adjusted model parameters. The CALIPSO aerosol-retrieval algorithm specifically uses attenuated backscatter and volume depolarization ratio coupled with surface type, layer, and altitude to determine the aerosol type (Fig. 6). The aerosol layers are identified by a set of algorithms known as selective iterative boundary locator (SIBYL) applied to 532-nm attenuated backscatter profiles. A scene classification algorithm

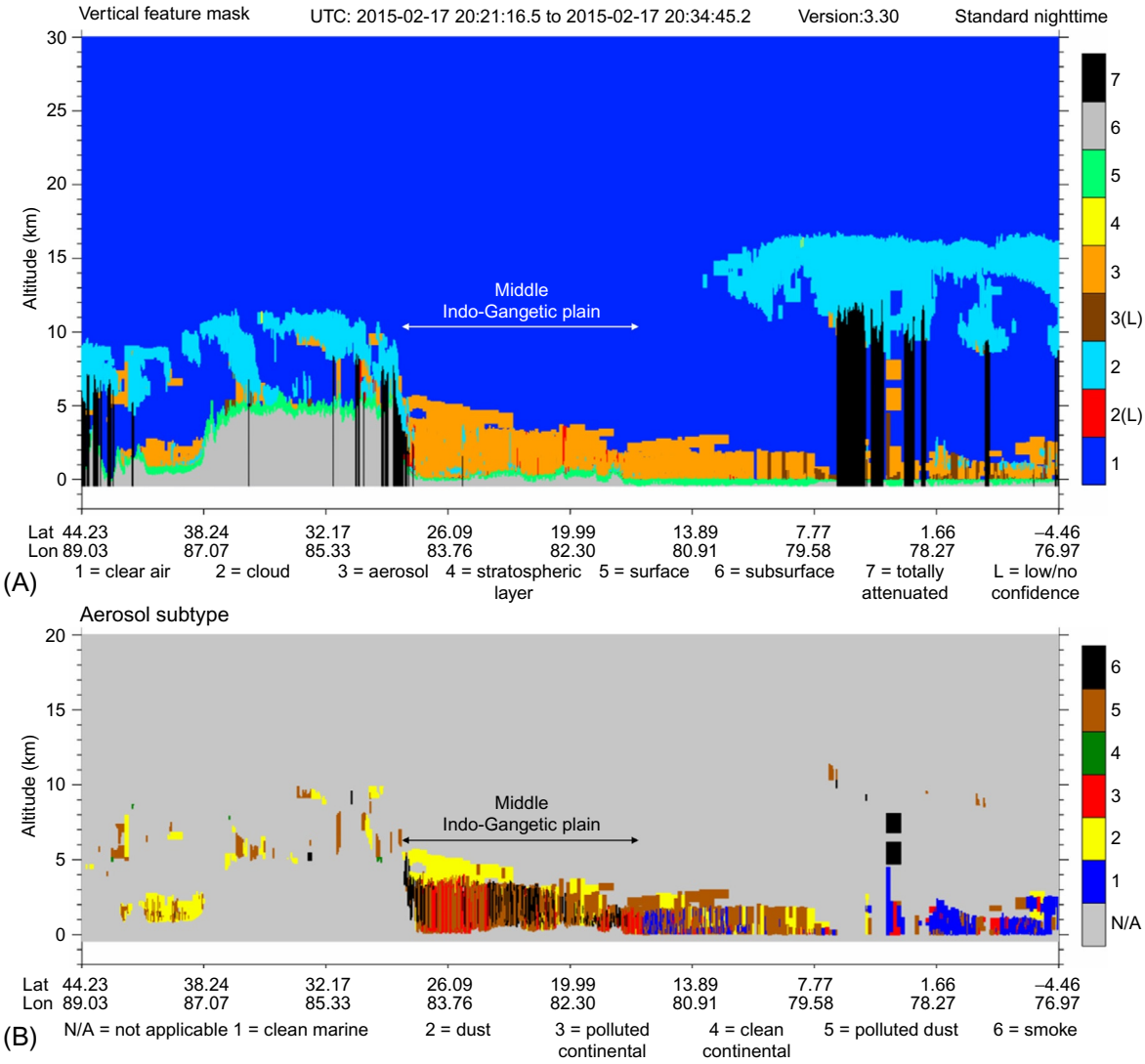

FIG. 6 CALIPSO profiles showing vertical distribution of aerosols, (A) vertical feature mask and (B) aerosol subtype.

(SCA) classifies the different layers of aerosols by type. Further, particle backscatter and extinction coefficients are retrieved using a hybrid extinction retrieval algorithm (HERA).

CALIPSO vertical profiles have been extensively used in atmospheric sciences, especially for studying various aerosol properties, their transport, sources, and radiative impacts. Yu et al. (2015) quantified trans-Atlantic dust transport from long-term CALIPSO LIDAR measurements. The study has estimated an outflow of nearly 182 Tga^{-1} dust per annum from the coast of North Africa. Observations taken by Ganguly et al. (2009) from multiple satellite instruments, including CALIPSO, confirmed the presence of huge amounts of aerosol haze over the Gangetic basin during winters. Over Bangkok, Bridhikitti (2013) recognized a uniform layer of smoke originating from biomass burning, resulting in high AOD over the entire region. Kumar et al. (2015a) used CALIPSO altitude-orbit cross-section profiles (level 2 version 3.30) to identify winter-specific nonspherical coarse particulates at relatively higher altitude and dominance of spherical fine particulates at lower altitude over the middle IGP (Fig. 6). In another study, Kumar et al. (2016) recognized the firework-specific emissions of aerosols and their vertical distribution over the middle IGP, which is reportedly dominated by smoke and polluted continental aerosols, especially at high altitudes (3.0–3.8 km).

5.5 Aerosol Properties From POLDER

Polarization and Directionality of the Earth's Reflectances (POLDER) is a passive optical imaging radiometer developed by CNES in collaboration with the LOA atmospheric optics laboratory in Lille, France. POLDER was designed to study cloud and aerosol properties in respect to climate systems. The first POLDER instrument was launched in August 1996 onboard an ADEOS-I satellite, which failed due to a technical error in June 1997. The next mission (POLDER 2) was launched in December 2002 aboard an ADEOS-II satellite; this, too, ended prematurely. The third-generation instrument was launched onboard PARASOL satellite in December 2004; this continued to operate until 2013. It measures the intensity, direction, and polarization of light reflected by the Earth and its atmosphere. POLDER scans between 443 and 1020 nm. Shorter wavelengths (i.e. 443–565 nm) are used to measure ocean color while longer wavelengths (670–1020 nm) are applied for studying vegetation and water vapor. POLDER is comprised of a two-dimensional CCD detector with a wide field view in cross-track (±51 degrees) and along-track (±43 degrees) directions (Deschamps et al., 1994). Polarization measurements are performed at 490, 670, and 0.865 nm. With an altitude of 705 km, it provides images of 2100 km × 1600 km resulting in global coverage within two days (Tanré et al., 2011).

Aerosol parameters are retrieved at 18.5 km × 18.5 km resolution using different algorithms over oceans and land. The inversion scheme developed by Deuzé et al. (1999) and Herman et al. (2005) was used to derive a number of parameters over oceans with dark surfaces in red and near IR spectral regions. The aerosol-retrieving algorithm utilizes the total and polarized radiances at 670 and 865 nm, assuming the size distribution follows two log-normal aerosol size distributions (reff < 0.5 μm and reff > 1.0 μm) with consideration of nonabsorbing particles in both modes. The total radiance (L) was given by:

$$L(\mu s, \mu v, \phi_v) = \eta L^f(\mu s, \mu v, \phi_v) + (1-\eta) L^c(\mu s, \mu v, \phi_v) \quad (15)$$

where η is the radiance weighting factor; $L^f(\mu s, \mu v, \phi_v)$ and $L^c(\mu s, \mu v, \phi_v)$ are the radiances of the fine (f) and coarse (c) modes, respectively; $\mu s = \cos(\theta_s)$ with θ_s the solar zenith angle; $\mu_v = \cos(\theta_s)$ for the viewing zenith angle; and ϕ_v the relative azimuth angle. The scattering by finer spherical particles generates highly

polarized light, which is better at estimating the presence of aerosols in comparison to total radiances. That is why only accumulation-mode aerosols are considered for the algorithm and coarser mode aerosols are ignored. Although there is almost no polarization from coarser aerosols, some misinterpretations could be made during extreme events that must be taken into account. The refractive index used is considered between 1.47 and 0.01 corresponding to aerosols from biomass burning or pollution events (Dubovik et al., 2002).

The aerosol retrievals from POLDER over oceans include total AOD, aerosol effective radius, the Angstrom exponent, finer AOD, and nonspherical AOD. Huang et al. (2015) studied the aspect ratios of Saharan and Asian dust using collocated MODIS Deep Blue product and the PARASOL level 2 Earth radiation. The mean aspect ratio for Saharan dust and two branches of Asian dust were reported as 2.5, 1.25, and 2.5, respectively. Apart from aerosols, POLDER data has also been widely used for multilayered cloud identifications.

5.6 Aerosol Properties From OMI

The Ozone Monitoring Instrument (OMI) is one of four sensors onboard the Aura satellite launched in July 2004. The OMI project is a joint effort by the Netherland Agency for Aerospace Program (NIVR), the Finnish Meteorological Institute (FMI), and NASA. It continues in the footprint of NASA's TOMS and ESA's GOME (Global Ozone Monitoring Experiment) instrumental records of atmospheric parameters and generates hyperspectral images by retrieving solar backscatter radiation in the visible and ultraviolet (UV) bands. The sun-synchronous orbit of OMI with a wide swath of 2600 km allows global coverage each day with a spatial resolution of 13×24 km at nadir and 28×150 km at the extreme of the view angle. The OMI measures the backscattering solar radiation from the earth's surface and atmosphere in multiple bands (270–500 nm). The key feature of OMI is the use of UV [UV-1 (270–314 nm), UV-2 (306–380 nm)], and the visible channel (350–500 nm) to measure backscatter radiation. Different algorithms have been used to retrieve data for various tropospheric air pollutants including ozone (O_3; both tropospheric and columnar), nitrogen dioxide (NO_2), sulfur dioxide (SO_2) and aerosols with the capability of distinguishing dust, smoke, and sulfates. It helps to detect volcanic ash, BrO, formaldehyde, and OClO and, thereby, plays an important role in understanding atmospheric chemistry.

For retrieving aerosols through OMI, two types of aerosol-retrieval algorithms are in use: the Near-UV aerosol algorithm (OMAERUV) and the Multi-Wavelengths Algorithm (OMAERO) having a pixel resolution of 13×24 km at nadir. The OMAERUV uses two UV wavelengths (354 and 388 nm) for retrieving aerosol extinction and absorption optical depth (AAOD), whereas the OMAERO is a multiwavelength algorithm having 19 channels (330–500 nm). The benefits of using the near-UV band include the ability to retrieve aerosol properties over a heterogeneous land surface even for highly bright surface areas. This primarily occurs because of relatively less surface reflectance over a bright land surface within the UV band. Using the near-UV band also enables OMI to retrieve absorbing aerosols (BC and desert dust) by utilizing the large sensitivity of these aerosols over the near-UV spectral band (Torres et al., 2007; Kumar et al., 2016). OMAERUV provides AOD, AAOD, and the aerosol index (AI) at two wavelengths (354 and 388 nm). However, due to cloud contamination, OMI AOD is often more reliable near the aerosol source under clear sky conditions while the AAOD is less affected by cloud contamination and, therefore, more reliable. The OMAERUV algorithm measures the Lambert Equivalent Reflectivity (LER) (Rx388) at 388 nm under the assumption that only

Rayleigh scattering occurs in the atmosphere and is surrounded by an opaque Lambertian reflector of reflectance Rx388 (Torres et al., 2007). The primary step of the OMAERUV algorithm is the calculation of the UV Aerosol Index (*UVAI*) (Torres et al., 2007):

$$UVAI = -100\log_{10}\left[\frac{I^{obs}_{354}}{I^{calc}_{354}\left(R^{*}_{354}\right)}\right] \qquad (16)$$

where I^{obs}_{354} is the TOA at 354 nm as observed by the sensor and I^{calc}_{354} is calculated by assuming an LER of (R^{*}_{354}). A multiwavelength algorithm (OMAERO) uses information over 19 spectral channels over near-UV and the visible wavelength to derive aerosol properties under cloud-free conditions (Fig. 7). At these spectral channels, Raman scattering and gas absorption occur only for the O_2-O_2 absorption band at

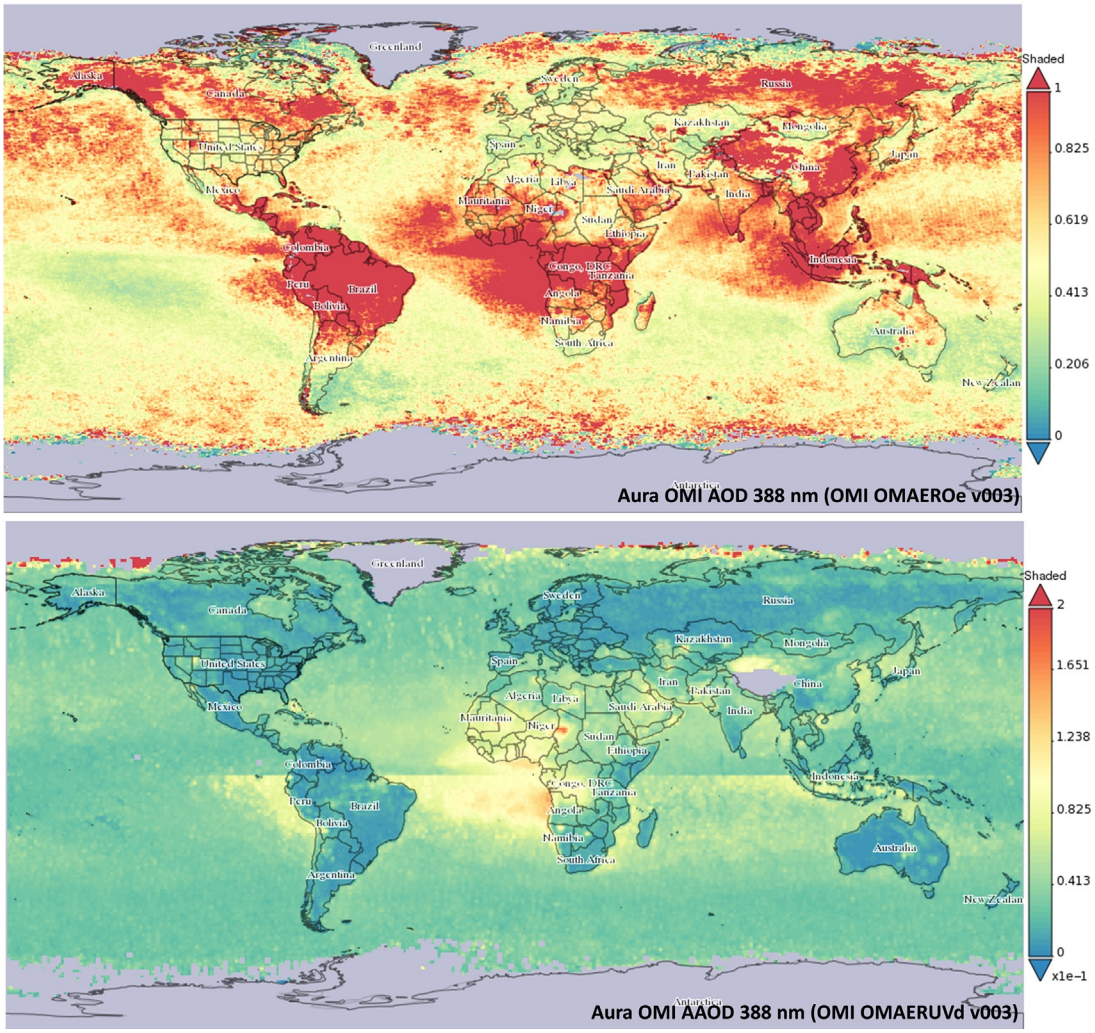

FIG. 7 Global variation of Aura OMI AOD and AAOD (at 388 nm) for 2015.

477 nm. The absorption band at 477 nm is used to enhance the sensitivity of the OMI reflectance measurement to aerosol layer and cloud height (Torres et al., 2007). Additionally, the inclusion of the near-UV band helps to separate weak and strong absorbing aerosols and therefore, functions better over the aerosol product from MODIS and MISR. The OMAERO algorithm provides AOD, aerosol type, SSA, aerosol layer height, and aerosol size distribution.

The OMI AOD and SSA retrievals have been previously compared with AERONET observations (Torres et al., 2007; Ahn et al., 2014). Both OMAERUV and OMAERO algorithms were also compared against MODIS (Curier et al., 2008) and MISR observations (Ahn et al., 2008), which reveal good agreement in terms of identifying major emission sources. Ahn et al. (2014) compared OMAERUV AOD with AERONET AOD at 44 sites globally and revealed that 65% of OMAERUV AOD agrees with AERONET AOD observations. The high sensitivity of OMI near-UV measurements to the absorption aerosols was used as complementary information on absorption aerosols when compared to MODIS and MISR. Curier et al. (2008) compared OMI-OMAERO and MODIS-retrieved AOD over Europe and surrounding oceans and concluded agreement between scenes both over ocean and land. Satheesh et al. (2009) used OMI-MODIS joint retrievals to improve the accuracy of retrieved aerosol products over the tropical North Atlantic. The results showed a good agreement between OMI and MODIS-predicted AODs in the UV range. Additionally, OMI has also been explored for retrieving trace gases around the world, like Shukla et al. (2017) used the Aura OMI-Differential Optical Absorption Spectroscopy (OMI-DOAS) algorithm to identify consistent and clear seasonal trends in the columnar ozone (2005–2015) with summertime maxima and wintertime minima over the middle IGP.

5.7 Aerosol Properties From VIIRS

The Visible Infrared Imaging Radiometer Suite (VIIRS) is a remote-sensing cross-track scanning radiometer onboard the Suomi National Polar-Orbiting Partnership (Suomi NPP) satellite. VIIRS was launched in October 2011 as a successor to AVHRR and MODIS, enabling a new generation of moderate resolution-imaging capabilities with high radiometric accuracy and spatial resolution. Using its 22 imaging and radiometric bands covering wavelengths from 0.41 to 12.5 μm, VIIRS accomplishes operational environmental monitoring and numerical weather forecasting. A dual-gain band allow VIIRS to retain high signal-to-noise ratio (SNR) at low radiance, thus making it suitable for concurrent application over land, ocean, and atmosphere. It has a scan width of about 3000 km (±56 degrees) allowing it to provide daily global coverage. VIIRS has an equator crossing time identical to MODIS (13:30 LT), with 86 seconds granule size having pixel resolution of 0.75 km at nadir and 1.5 km at edge (Jackson et al., 2013). VIIRS uses three different bands—imagery, moderate resolution (M-bands), and the day-night band—and its main products include clouds, sea surface temperature, ocean color, polar wind, vegetation, aerosol, fire, snow, and ice. The primary aerosol data include AOD and aerosol type retrieved mainly between 412 and 2250 nm. The VIIRS retrieved AOD at 388 nm is shown in Fig. 8, which closely resembles the MODIS-derived AOD over the same region (Fig. 4).

VIIRS aerosol retrievals are made over M-bands (0.412–12.016 μm) while AOD is specifically retrieved at 550 nm. It has the capability of retrieving the Angstrom exponent and aerosol type over land and can distinguish aerosol fine and coarse mode fractions over ocean (Jackson et al., 2013). The level 2 product of VIIRS available for end users is designated as the environmental data record (EDR), which includes aerosol optical thickness (AOT), the

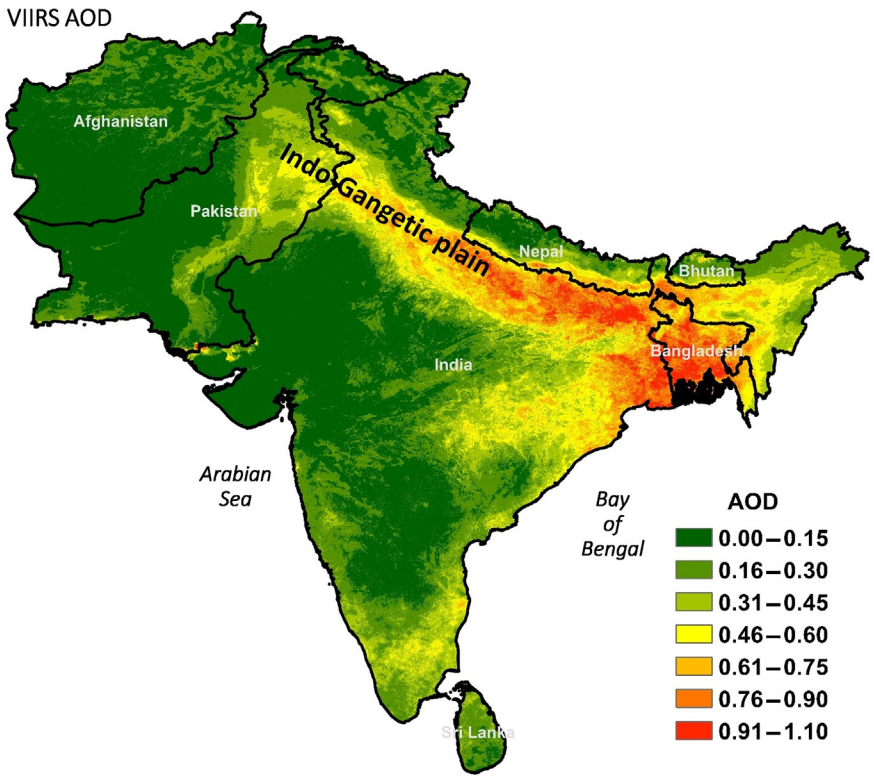

FIG. 8 Winter-specific columnar AOD (at 388 nm) over South Asia retrieved from VIIRS.

aerosol particle size parameter (APSP), and suspended matter (SM). The SM EDR includes classification of aerosol types with categories including crustal dust, smoke, volcanic ash, and sea salt. However, aerosol retrieval is performed only during daytime for cloud-free pixels and over dark land surfaces. The aerosol algorithm of VIIRS mostly resembles the MODIS collection 3 algorithm (Kaufman et al., 1997; Tanré et al., 1997) with specific changes over land. The algorithms over ocean also have some modifications in comparison to their MODIS counterpart. The VIIRS algorithm pursues an approximation of vector radiation transfer model (RTM) version 1.1 (6S-V1.1) (Kotchenova and Vermote, 2007). The spectral reflectance measured at satellite level $\rho_{toa}(\tau_A)$ is calculated using the equation:

$$\rho_{toa}(\tau_A) = \mathrm{Tg_{og}TgO_3}\left[\rho_A(\tau_A)\mathrm{TgH_2O(UH_2O/2)} + \rho_R(P) + \mathrm{TgH_2O(UH_2O)}\cdot\left\{T_{R+A}(\tau_A,\theta_s)(T_{R+A}(\tau_A,\theta_v)\frac{\rho_{\mathrm{surf}}}{1-S_{R+A},\rho_{\mathrm{surf}}} + (\text{nonlambertian terms})\right\}\right] \quad (17)$$

where τ_A is AOT; θ_s and θ_v are the solar and view zenith angles, respectively; P is surface pressure; ρ_R and ρ_A denote the atmospheric path reflectance due to molecular and aerosol scattering; T_{r+a} is the total transmittance attributed to molecules and aerosols; $\mathrm{TgO_3}$ and $\mathrm{TgH_2O}$ are transmittances from ozone and water vapor, respectively; $\mathrm{UH_2O}$ represents total columnar water vapor; $\mathrm{Tg_{og}}$ is the two-way transmittance from O_2, CO_2, CH_4, and N_2O); ρ_{surf} is the Lambertian surface reflectance; and S_{r+a} is the spherical albedo of the atmosphere.

A number of assumptions have been made for the calculation of spectral reflectance, which can be found elsewhere (Jackson et al., 2013). The reflectance in 412, 445, 488, 672, and 2250 nm bands have been used for aerosol retrievals over land. The land inversion approach used for retrieving AOD utilized an empirically derived relationship between surface reflectance in 488 and 672 nm bands. Reflectance in other bands is used for choosing an appropriate model among a set of candidates. The change in ratio of the TOA reflectance in the blue and red bands from the surface value in the presence of aerosols is the primary basis of AOD retrieval over land.

The accuracy of global VIIRS AOD has been evaluated in comparison to MODIS, AERONET, and the Maritime Aerosol Network (MAN) by Liu et al. (2014). A slight difference between VIIRS global mean AOD at 550 nm from MODIS AOD was recorded at 0.01 and 0.03 over ocean and land, respectively. Validation with AERONET and MAN measurements experienced biases of 0.01 over ocean and 0.01 over land. Similar efforts of validating global VIIRS AOD with AERONET AOD by Huang et al. (2016) exhibited an overall bias of 0.02 over oceans and −0.0008 over land. Meng et al. (2015) on the other hand reported the spatiotemporal variability of VIIRS AOD over China and observed a difference of –0.0032 from MODIS-derived AOD. Oliva and Schroeder (2015) applied the VIIRS 375 fire-detection product to assess its performance for direct burned area estimation for different ecologically sensitive areas. The results were compared with Landsat-8 supervised burned area classification and a higher accuracy was observed in forests with fires of a lengthy duration. However, errors were reported over grasslands, savannas, and agricultural areas. The limitations of MODIS AOD in terms of nonavailability of nighttime AOD for air-quality studies can be compensated by using the VIIRS day/night band. Wang et al. (2016) showed quantitative changes in the intensity of light during night that can reflect the variations in surface $PM_{2.5}$. Other prominent applications of VIIRS-based retrievals include estimation of chlorophyll-a based on ocean color index (Wang and Son, 2016) as well as validation of land surface temperature (Guillevic et al., 2014) and sea surface temperature (Gladkova et al., 2015).

5.8 Aerosol Properties From OCM

The Oceansat satellite was launched by the Indian Space Research Organisation (ISRO). The Oceansat-2 OCM (Ocean Colour Monitor) sensor, launched in 2009, is the successor to the Oceansat-1 OCM. The sensor details are provided in Table 2. The OCM sensor is designed for ocean color studies. The spectral bands of the Oceansat-1 OCM sensor were similar to those of the SeaWiFS sensor, while the Oceansat-2 OCM sensor is identical to the Oceansat-1 OCM sensor except in bands 6 and 7. Band 6 of Oceansat-1 had an effective wavelength at 670 nm, and for Oceansat-2, it shifted to 620 nm. This change was made to improve the quantification of suspended sediment concentration. Band 7 of Oceansat-1 had an effective wavelength at 765 nm, which was shifted to 745 nm for Oceansat-2 in order to avoid oxygen absorption. The overview of sensor details is given in Nagamani et al. (2008). Oceansat-2 acquires the data every two days at a spatial resolution of 360 m. The OCM sensor has been used for studying ocean phytoplankton, suspended sediments, and AOD over the ocean by many researchers (Nagamani et al., 2008; Mishra et al., 2008). In addition to its capability of studying the ocean surface, the OCM sensor also has the potential to study land surface features. Studies on coastal mangroves and NDVI have been carried out using the OCM Sensor (Nayak et al., 2001). The enhanced vegetation

TABLE 2 Oceansat-2 Bands, Effective Wavelength and Extraterrestrial Solar Radiation

Oceansat 2 (OCM) Bands	Wavelength Range (μm)	Effective Wavelength (μm)	Extraterrestrial Solar Radiation ($Wm^{-2}\mu m^{-1}$) ($\bar{E}_0$)
Band-1	0.402–0.422	0.412	1728.15
Band-2	0.433–0.453	0.443	1852.11
Band-3	0.480–0.500	0.490	1972.10
Band-4	0.500–0.520	0.510	1866.97
Band-5	0.545–0.565	0.555	1827.81
Band-6	0.610–0.630	0.620	1657.65
Band-7	0.725–0.755	0.740	1289.70
Band-8	0.845–0.885	0.865	952.073

index (EVI) has been retrieved from the OCM Sensor (Mishra and Dadhwal, 2008; Mishra, 2014).

The first step for retrieval of AOD from Oceansat-2 is to identify the high-reflecting pixels like clouds and snow in the image. In the absence of a thermal band, a threshold approach can be adopted for identifying the cloud-and snow-contaminated pixels. The second step is to differentiate the pixel of the image as vegetated and sparsely vegetated or a sand-dominated pixel based on the NDVI value. The surface reflectance of the pixel with NDVI value >0.1 can be determined following the approach by Hsu et al. (2013). The surface reflectance values for the pixel having NDVI values <0.1 can be determined following the procedure provided by von Hoyningen-Huene et al. (2003). However, surfaces having sparse or no vegetation need further approximation using statistical interpolation and the spectral relationship of white sand (Ouillon et al., 2002). The AOD derived from the Oceansat-2 can be used along with Terra- and Aqua-derived AOD to study the diurnal variation. The AOD over densely populated areas can be correlated with the concentrations of fine particulate matter.

6 AEROSOL REMOTE SENSING OVER THE INDO-GANGETIC PLAIN, SOUTH ASIA

The Indo-Gangetic Plain (IGP) has always been a center of discussion when it comes to air quality. Being a highly populated and fertile region starting from the plains of the Indus River over Pakistan to the Bay of Bengal over India, it covers an area of 255 million hectares of land. The presence of a huge number of polluting sources—industries (Banerjee et al., 2011), domestic biomass burning (Murari et al., 2016; Sen et al., 2016, 2017), high vehicular density with limited emission control (Murari et al., 2015), open refuse and waste burning practices (Banerjee and Srivastava, 2012; Banerjee et al., 2017b) and resuspension of crustal dusts (Banerjee et al., 2015)—are some common sources of air pollution. Additionally, the post-harvest burning of agricultural residue (Rastogi et al., 2016) and transboundary movement of aerosols (Kumar et al., 2015b, 2017; Sen et al., 2017) substantiate regional pollution loading. Due to the limited ground-based aerosol monitoring network, satellite remote sensing has long been used to measure the spatiotemporal variation of aerosols and the climatic impact

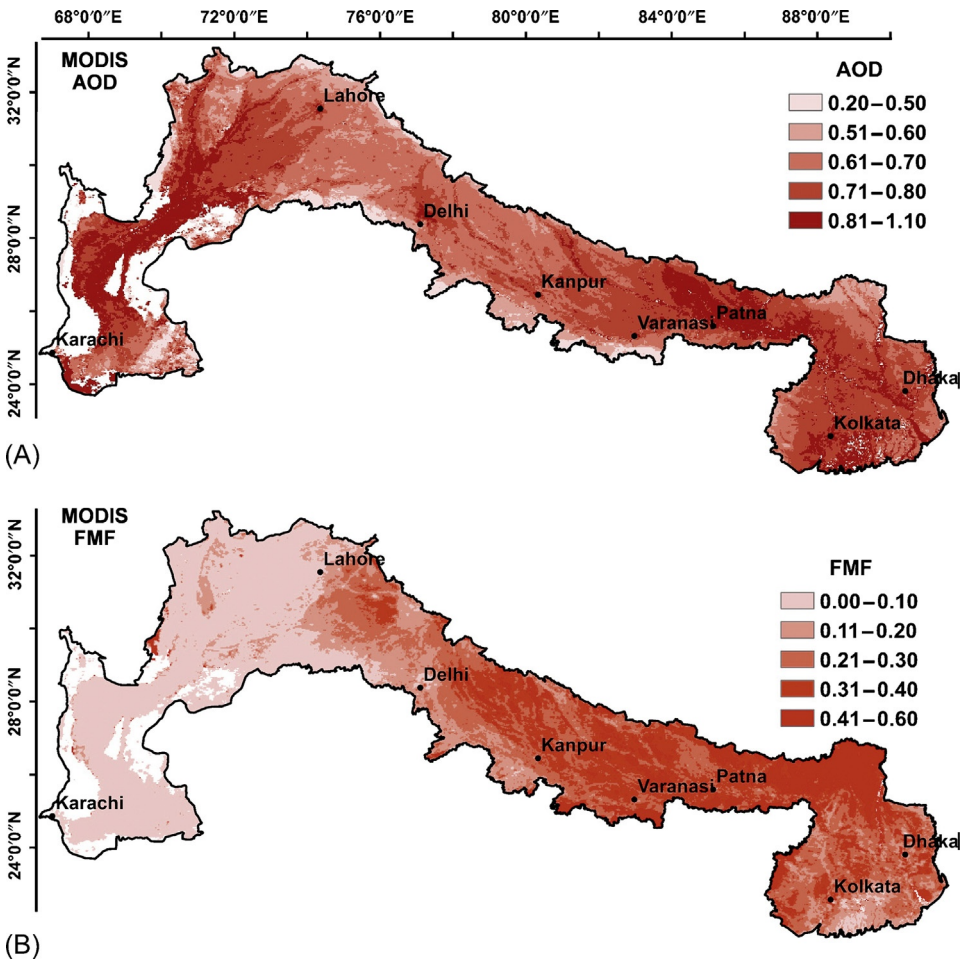

FIG. 9 Comparative figures of mean (2011–2015) Terra MODIS, (A) AOD and (B) FMF over the Indo-Gangetic Plain.

over the region. Fig. 9 represents the characteristic variation of AOD for 2 years (2014–2015; Fig. 9A) with corresponding FMFs over the entire IGP (Fig. 9B). Both the upper and middle IGP exhibit a high columnar aerosol loading while the prevalence of FMF is quite diverse. Relatively high coarser particulate loading was recognized over the upper IGP while dominance of fine particulates is only evident in the lower region. Several case studies (Table 3) on aerosol remote sensing over the IGP have documented the contribution of crustal sources (Banerjee et al., 2015) and biomass burning for aerosol emission (Rastogi et al., 2016; Kaskaoutis et al., 2014; Vadrevu et al., 2011), variation in aerosol composition (Kumar et al., 2015b, 2017; Singh et al., 2017a), estimation of surface $PM_{2.5}$ using satellite observation (Dey et al., 2012), and estimating aerosol radiative forcing (Dey and Tripathi, 2007; Kumar et al., 2017) over the region. For the following subsection, emphases were made to discuss some major conclusions on aerosol properties retrieved through satellite remote sensing over the entire IGP.

TABLE 3 Aerosol Remote Sensing Over the Indo-Gangetic Plain, South Asia

Location	Type of Study	Satellite Aerosol Parameters Used	References
Lahore	Trend analysis	MODIS-AOD	Gupta et al. (2013)
Patiala	Biomass burning event	MODIS-AOD, MODIS-Active Fire Count, OMI-Aerosol Index	Sharma et al. (2014)
Hisar	Source-specific radiative forcing	MODIS-AOD	Raman et al. (2011)
New Delhi	AOD-PM relation	MODIS-AOD	Kumar et al. (2007)
New Delhi	Aerosol characteristics and radiative forcing	MODIS-AOD, MISR-AOD, CALIPSO-Extinction Coefficient	Srivastava et al. (2014)
Agra	AOD-PM relation	MODIS-AOD	Chitranshi (2015)
Kanpur	Aerosol climatology	MODIS-AOD, MISR-AOD	Prasad and Singh (2007)
Allahabad	Fog event	MODIS-False color composite	Badarinath et al. (2011)
Varanasi	AOD-PM relation	MODIS-AOD	Kumar et al. (2015b)
Varanasi	Temporal variation	MODIS-AOD	Tiwari and Singh (2013)
Varanasi	Fireworks event	MODIS-AOD, Fine-Mode Fraction, CALIPSO-Extinction Coefficient, Backscatter profiles	Kumar et al. (2016)
Patna	Aerosol climatology	MODIS-AOD	Ramachandran et al. (2012)
Kolkata	Temporal variation	MODIS-AOD, MISR-AOD	Mehta (2015)
Dhaka	Temporal variation	MODIS-AOD	Mamun et al. (2014)

A long-term decadal assessment of MODIS-based aerosol distribution was made by Ramachandran et al. (2012) throughout India, including selected stations over the IGP. MODIS Terra level-2 AOD was used to delineate their season-specific trends. An increasing trend of AOD at a few stations such as New Delhi depicted the upsurge of anthropogenic sources of pollution, including fossil fuel- and biomass-burning activities. Prasad and Singh (2007) also reported similar evidence of increasing satellite-derived (MODIS and MISR) aerosol loading during 2000–2005 over major cities of the IGP. Studies clearly indicate the impact of natural sources and anthropogenic activities, especially biomass burning, resulting in different climatic implications. The long-term indirect effects of the aerosol burden on water and the ice-cloud effective radius were assessed by Tripathi et al. (2007) using MODIS-derived AOD. The intensity of indirect effects for clouds were reported highest during winter while its spatial extent was reported maximum during monsoon.

Post-harvest specific agro-residue burning is an important event that critically affects air quality over the IGP. Remote-sensing techniques have been extensively used to study the biomass burning evidence and its impact on regional air quality. Vadrevu et al. (2011) highlighted the remotely sensed fire products and their potential to characterize the agricultural residue burning events and their impacts on air quality.

The assessment of fire counts from MODIS data revealed the bimodal activities in fire intensity, fire radiative energy, and optical depths pertaining to wheat and rice residue burning. Kaskaoutis et al. (2014), using a synergy of both ground-based and satellite observations (MODIS and OMI), evaluated the impacts of rice residue burning over northern India postmonsoon and found evidence that it generated a thick aerosol layer (below 2–2.5 km) over the IGP. Strong AOD gradients during postharvest were also observed before subsequently being transported from the upper to lower Gangetic basin. Sharma et al. (2010) established significant impacts of crop residue burning on aerosol properties using ground as well as multisatellite data with high AOD and Angstrom exponent values. In a recent review on organic aerosols over the IGP, Singh et al. (2017b) concluded the contribution of biomass burning, especially crop residue burning over the upper IGP, which contribute massive aerosol loading to both the middle and lower IGP regions through long-range transport. Similar findings have also been reported by Sen et al. (2017) recognizing the long-range transport of aerosols from the upper IGP and IHP region to the Bay of Bengal, thereby potentially intruding upon the cloud formation process.

Estimation of near-surface particulates using satellite-retrieved data is one of the foremost applications of aerosol remote sensing. Based on the highly heterogeneous nature of aerosols over the IGP and uneven meteorological conditions throughout the year, it is quite a challenging task for researchers. Dey et al. (2012), using MISR-retrieved AOD, estimated surface $PM_{2.5}$ for the Indian subcontinent accounting for both composition and aerosol vertical distribution. The study revealed the exposure of nearly 51% of the subcontinent's population to high airborne particulate concentration. Interestingly, some rural areas were reported to have higher aerosol loading compared to urban areas. Relation between MODIS AOD and surface $PM_{2.5}$ in New Delhi was reported by Kumar et al. (2007). The empirical estimation of near-surface aerosol masses using satellite-based AOD appears to be helpful. However, it is quite complicated over the IGP with varying sources and meteorological conditions. Exemplifying range of association ($r = 0.46$–0.54) between AOD and near-surface particulates was reported by Kumar et al. (2015b) during winter.

Satellite-retrieved information has opened up a new way of characterizing aerosol subtypes with distinct spatial and vertical resolution. Several studies have been reported over the IGP using remote-sensing techniques to identify various aerosol types. Using CALIPSO-based measurements, Kumar et al. (2015a,b) identified a variety of aerosol layers at different altitudes over the middle IGP. A sharp deviation and episodic nature were reported in the aerosol subtypes that clearly indicate the dominance of different sources. The application of prevailing air masses for the classification of aerosol types was made by Tiwari et al. (2015) at Varanasi on the basis of cluster analysis of air mass. The contribution of polluted dust, polluted continental, and black and organic carbon-enriched aerosols were mainly observed at the central part of the IGP, which highlights the extent of human-induced pollution over the region. Aerosol extinction properties were used by Verma et al. (2016) to categorize the possible aerosol subtypes at the lower Gangetic basin. They reported the influence of dust and polluted dust during daytime whereas polluted continental and smoke during nighttime. Srivastava et al. (2014) reported the presence of dust over the national capital of Delhi throughout the year, with an aerosol layer mostly confined within 2 km during winter and postmonsoon before elevating to 6 km during premonsoon and monsoon seasons.

Some extreme events like dust storms, haze, and fog over the IGP are tracked using remote-sensing techniques. Northern India usually experiences premonsoon dust storms that

significantly modify the regional aerosol characteristics for a shorter period of time. Kumar et al. (2014), using WRF-Chem simulations based on MODIS and AERONET retrievals, observed an increase (>50%) in local-to-regional AOD and a decrease (>70%) in the AE during a pre-monsoon dust storm. The study on aerosol radiative impacts during the dust storm showed a cooling effect at the surface and top of the atmosphere, while warming the atmosphere. Kumar et al. (2016) used MODIS-AOD and CALIPSO aerosol vertical profiles to identify fireworks-induced particulate pollution over the entire Indian region. These case studies referring to the application of satellite remote sensing for studying aerosol characteristics, distribution, transport, and radiative impacts over the IGP provide extremely useful information on aerosol-induced climate and air quality changes over the region.

7 CONCLUSIONS AND FUTURE PROSPECTS

Retrieval of aerosol optical properties from satellite-based remote sensing has been used most efficiently to complement ground-based measurements and to link aerosol properties with climate change. Although retrieval of aerosol microphysical properties from satellite-based sensors is relatively new, it poses the potential to provide a generic description of existing atmospheric profiles. Application of remote-sensing techniques has emerged with several advantages like large spatial coverage, real-time data, reliability, the use of multiple platforms, and the identification of aerosol properties with varying vertical resolutions. With multiple validation and an intercomparison network, remote-sensing information has emerged with much more reliability and, thereby, provides a scope of extensive applications in multidisciplinary fields. There are numerous examples of the successful application of satellite-retrieved aerosol properties in identifying transboundary movement, aerosol source and receptors, variation in particle morphology, physiochemical properties, and computing radiative impacts both in the TOA and at surface.

Further, numerous satellites have been launched with a diverse field of applications under a common platform with near-simultaneous observations to provide a holistic view of the entire atmosphere. Likewise, NASA's international Afternoon Constellation (A-Train), including OCO-2, GCOM-W1, Aqua, CALIPSO, CloudSat, and Aura, provide near-simultaneous observation of multiple parameters related to cloud, aerosol, trace gases, and other climate variables. Additionally, some application-based satellites are also in line to be launched. For example, ESA's EarthCARE satellite is scheduled to be launched in 2018 and is expected to advance our understanding on aerosol-cloud interaction using high-performance LIDAR and radar technology. The Earth Explorer Atmospheric Dynamics Mission (ADM-Aeolus) will provide global observations of wind to improve weather forecasts. The Sentinel series is focusing on retrieving trace gas and aerosol properties with improved near-real time monitoring. There are few overambitious projects scheduled to be launched under Earth observing system. Most notably, the Stratospheric Aerosol and Gas Experiment (SAGE III) on the International Space Station; the Geostationary Coastal and Air Pollution Events (GEO-CAPE) for identifying natural and anthropogenic sources of aerosols; the Aerosol-Cloud-Ecosystems (ACE) for measuring aerosol and cloud types and properties; the Global Atmosphere Composition Mission (GACM) for ozone and related gases for intercontinental air quality; the Pre-Aerosol, Clouds, and Ocean Ecosystem (PACE) for extended data records on clouds and aerosols (http://eospso.nasa.gov/future-missions): and the Tropospheric Emissions: Monitoring of Pollution (TEMPO) for ozone precursors, aerosols,

and clouds. The TEMPO (for North America) will further be a part of the global air quality monitoring constellation, including GEMS (Geostationary Environment Monitoring Spectrometer) for Asia-Pacific and Sentinel-4 for Europe. The NEMO (Next-Generation Earth Monitoring and Observation) bus will be the next evolution to the Generic Nanosatellite Bus (GNB) technology jointly developed by the Indian Space Research organization (ISRO) and the Space Flight laboratory at the University of Toronto to provide information on aerosol and earth systems. Another flagship project called the Multi-Angle Imager for Aerosols (MAIA) is scheduled to be launched by NASA in January 2020. MAIA is a multiview satellite sensor, currently under development by NASA's Earth Science Division. It contains two push-broom spectropolarimetric cameras capable of measuring radiance in 12 spectral bands. This will help to provide information on aerosol loading, size, and compositions at much finer scale and thereby has potential for broader applications like assessing the impact of aerosols on human health, agricultural productivity, and hydrological cycles.

Therefore, it may well be projected that the use of satellite-retrieved aerosol properties for applications in climate and ambient air quality will be further developed in near future. This will further improve our knowledge on earth, the atmosphere and climate. Observations of atmospheric aerosols and trace gases from satellite sensors will be combined with health information to determine the toxicity of airborne particulates and the subsequent development of a sustainable habitat. Consequently, the availability of near real-time remote sensing data will precisely help in air quality forecasting and developing an effective health-advisory service.

Acknowledgments

The authors are grateful to the agencies that provided the satellite data on the earth system's science. Authors wish to acknowledge Terra/Aqua-MODIS and VIIRS data from NASA's LAADS Web, Terra-MISR from ASDC/NASA, CALIPSO-CALIOP from Atmospheric Science Data Center at NASA Langley Research Center, Aura-OMI data from GES DISC, and OCM-Oceansat-2 from ISRO. Additionally, the authors also wish to thank all the scientists who have devoted their life to developing remote-sensing science.

References

Ackerman, S.A., Strabala, K.I., Menzel, W.P., Frey, R.A., Moeller, C.C., Gumley, L.E., 1998. Discriminating clear sky from clouds with MODIS taken from the MAS during the SUCCES experiment. J. Geophys. Res 103 (D24), 32141–32157.

Ahn, C., Torres, O., Bhartia, P.K., 2008. Comparison of ozone monitoring instrument UV aerosol products with Aqua/Moderate Resolution Imaging Spectroradiometer and Multiangle Imaging Spectroradiometer observations in 2006. J. Geophys. Res. 113 (D16), 1–13.

Ahn, C., Torres, O., Jethva, H., 2014. Assessment of OMI near-UV aerosol optical depth over land. J. Geophys. Res. Atmos. 119 (5), 2457–2473.

Albrecht, B., 1989. Aerosols, cloud microphysics, and fractional cloudiness. Science 245, 1227–1230.

Angstrom, A., 1964. The parameters of atmospheric turbidity. Tellus 16, 64–75.

Badarinath, K.V.S., Kharol, S.K., Chand, T.K., Latha, K.M., 2011. Characterization of aerosol optical depth, aerosol mass concentration, UV irradiance and black carbon aerosols over Indo-Gangetic plains, India, during fog period. Meteorol. Atmos. Phys. 111 (1–2), 65–73.

Banerjee, T., Srivastava, R.K., 2012. Plastics waste management and resource recovery in India. Int. J. Environ. Waste Manag. 10 (1), 90–111.

Banerjee, T., Barman, S.C., Srivastava, R.K., 2011. Application of air pollution dispersion modeling for source-contribution assessment and model performance evaluation at integrated industrial estate-Pantnagar. Environ. Pollut. 159, 865–875.

Banerjee, T., Murari, V., Kumar, M., Raju, M.P., 2015. Source apportionment of airborne particulates through receptor modeling: Indian scenario. Atmos. Res. 164–165, 167–187.

Banerjee, T., Kumar, M., Singh, N., 2017a. Aerosol, climate and sustainability. In: Reference Module in Earth Systems and Environmental Sciences. Encyclopaedia of Anthropocene, Elsevier. https://doi.org/10.1016/B978-0-12-409548-9.09914-0.

Banerjee, T., Kumar, M., Mall, R.K., Singh, R.S., 2017b. Airing 'clean air' in Clean India Mission. Environ. Sci. Pollut. Res. 24 (7), 6399–6413.

Bevan, S.L., North, P.R.J., Grey, W.M.F., Los, S.O., Plummer, S.E., 2009. Impact of atmospheric aerosol

from biomass burning on Amazon dry-season drought. J. Geophys. Res. Atmos. 114 (D9).
Bevan, S.L., North, P.R.J., Los, S.O., Grey, W.M.F., 2012. A global dataset of atmospheric aerosol optical depth and surface reflectance from AATSR. Remote Sens. Environ. 116, 199–210.
Bibi, H., Alam, K., Chishtie, F., Bibi, S., Shahid, I., Blaschke, T., 2015. Intercomparison of MODIS, MISR, OMI, and CALIPSO aerosol optical depth retrievals for four locations on the Indo-Gangetic plains and validation against AERONET data. Atmos. Environ. 111, 113–126.
Bridhikitti, A., 2013. Atmospheric aerosol layers over Bangkok Metropolitan Region from CALIPSO observations. Atmos. Res. 127, 1–7.
Che, H.Z., Wang, Y.Q., Sun, J.Y., Zhang, X.C., Zhang, X.Y., Guo, J.P., 2013. Variation of aerosol optical properties over the taklimakan desert in China. Aerosol Air Qual. Res. 13, 777–785.
Chin, M., Ginoux, P., Kinne, S., Torres, O., Holben, B.N., Duncan, B.N., Martin, R.V., Logan, J.A., Higurashi, A., Nakajima, T., 2002. Tropospheric aerosol optical thickness from the GOCART model and comparisons with satellite and sun photometer measurements. J. Atmos. Sci. 59, 461–483.
Chitranshi, S., Sharma, S.P., Dey, S., 2015. Satellite-based estimates of outdoor particulate pollution (PM10) for Agra City in northern India. Air Qual. Atmos. Health 8 (1), 55–65.
Corbett, J.J., Winebrake, J.J., Green, E.H., Kasibhatla, P., Eyring, V., Lauer, A., 2007. Mortality from ship emissions: a global assessment. Environ. Sci. Technol. 41 (24), 8512–8518.
Curier, R.L., Veefkind, J.P., Braak, R., Veihelmann, B., Torres, O., 2008. Retrieval of aerosol optical properties from OMI radiances using a multiwavelength algorithm: application to Western Europe. J. Geophys. Res. Atmos. 113, 1–16.
Das, S., Dey, S., Dash, S., 2014. Impacts of aerosols on dynamics of Indian summer monsoon using a regional climate model. Clim. Dynam. 44, 1685–1697.
De Leeuw, G., Schoemaker, R., Curier, L., Bennouna, Y., Timmermans, R., Schaap, M., Koelemeijer, R., 2007. AATSR derived aerosol properties over land. In: ENVISAT Symposium, ESA SP-636, July.
Deschamps, P.Y., Buriez, J.C., Bréon, F.M., Leroy, M., Podaire, A., Bricaud, A., Sèze, G., 1994. The POLDER mission: instrument characteristics and scientific objectives. IEEE Trans. Geosci. Remote Sens. 32 (3), 598–615.
Deuzé, J.L., Herman, M., Goloub, P., Tanré, D., Marchand, A., 1999. Characterization of aerosols over ocean from POLDER/ADEOS-1. Geophys. Res. Lett. 26 (10), 1421–1424.
Dey, S., Tripathi, S.N., 2007. Estimation of aerosol optical properties and radiative effects in the Ganga basin, northern India, during the wintertime. J. Geophys. Res. Atmos 112 (D3), 1–16.
Dey, S., Di Girolamo, L., van Donkelaar, A., Tripathi, S.N., Gupta, T., Mohan, M., 2012. Variability of outdoor fine particulate ($PM_{2.5}$) concentration in the Indian subcontinent: a remote sensing approach. Remote Sens. Environ. 127, 153–161.
Dubovik, O., Holben, B., Eck, T.F., Smirnov, A., Kaufman, Y.J., King, M.D., Tanré, D., Slutsker, I., 2002. Variability of absorption and optical properties of key aerosol types observed in worldwide locations. J. Atmos. Sci. 59 (3), 590–608.
Dubovik, O., Lapyonok, T., Kaufman, Y., Chin, M., Ginoux, P., et al., 2007. Retrieving global sources of aerosols from MODIS observations by inverting GOCART model. Atmos. Chem. Phys. Discuss. 7 (2), 3629–3718.
Evans, J., van Donkelaar, A., Martin, R.V., Burnett, R., Rainham, D.G., Birkett, N.J., Krewski, D., 2013. Estimates of global mortality attributable to particulate air pollution using satellite imagery. Environ. Res. 120, 33–42.
Fang, H., Liang, S., Hoogenboom, G., 2011. Integration of MODIS LAI and vegetation index products with the CSM–CERES–Maize model for corn yield estimation. Int. J. Remote Sens. 32 (4), 1039–1065.
Fraser, R.S., Kaufman, Y.J., Mahoney, R.L., 1984. Satellite measurements of aerosol mass and transport. Atmos. Environ. 18, 2577–2584.
Ganguly, D., Ginoux, P., Ramaswamy, V., Winker, D.M., Holben, B.N., Tripathi, S.N., 2009. Retrieving the composition and concentration of aerosols over the Indo-Gangetic basin using CALIOP and AERONET data. Geophys. Res. Lett. 36 (13), 1–5.
Gladkova, I., Kihai, Y., Ignatov, A., Shahriar, F., Petrenko, B., 2015. SST Pattern Test in ACSPO clear-sky mask for VIIRS. Remote Sens. Environ. 160, 87–98.
Griggs, M., 1975. Measurements of atmospheric aerosol optical thickness over water using ERTS-1 data. J. Air Pollut. Control. Assoc. 25, 622–626.
Guenther, B., Xiong, X., Salomonson, V.V., Barnes, W.L., Young, J., 2002. On-orbit performance of the earth observing system moderate resolution imaging spectroradiometer; first year of data. Remote Sens. Environ. 83 (1–2), 16–30.
Guillevic, P.C., Biard, J.C., Hulley, G.C., Privette, J.L., Hook, S.J., Olioso, A., Csiszar, I., 2014. Validation of land surface temperature products derived from the visible infrared imaging radiometer suite (VIIRS) using ground-based and heritage satellite measurements. Remote Sens. Environ. 154, 19–37.
Gupta, P., Christopher, S.A., Box, M.A., Box, G.P., 2007. Multiyear satellite remote sensing of particulate matter

air quality over Sydney, Australia. Int. J. Remote Sens. 28 (20), 4483–4498.
Gupta, P., Khan, M.N., da Silva, A., Patadia, F., 2013. MODIS aerosol optical depth observations over urban areas in Pakistan: quantity and quality of the data for air quality monitoring. Atmos. Pollut. Res. 4 (1), 43–52.
Hansen, J., Sato, M., Ruedy, R., 1997. Radiative forcing and climate response. J. Geophys. Res. 102, 6831–6864.
Herman, M., Deuzé, J.L., Marchand, A., Roger, B., Lallart, P., 2005. Aerosol remote sensing from POLDER/ADEOS over the ocean: Improved retrieval using a nonspherical particle model. J. Geophys. Res. D: Atmos. 110 (10), 1–11.
Holben, B.N., Eck, T.F., Slutsker, I., Tanré, D., Buis, J.P., Setzer, A., Vermote, E., 1998. AERONET—a federated instrument network and data archive for aerosol characterization. Remote Sens. Environ. 66 (1), 1–16.
Hsu, N.C., Tsay, S.-C., King, M.D., Herman, J.R., 2004. Aerosol properties over bright-reflecting source regions. IEEE Trans. Geosci. Remote Sens. 42 (3), 557–569.
Hsu, N.C., Tsay, S., King, M.D., Member, S., Herman, J.R., During, A., 2006. Deep blue retrievals of Asian aerosol properties during ACE-Asia. IEEE Trans. Geosci. Remote Sens. 44 (11), 3180–3195.
Hsu, N.C., Jeong, M.J., Bettenhausen, C., Sayer, A.M., Hansell, R., Seftor, C.S., Tsay, S.C., 2013. Enhanced deep blue aerosol retrieval algorithm: the second generation. J. Geophys. Res. Atmos. 118 (16), 9296–9315.
Hu, Z., 2009. Spatial analysis of MODIS aerosol optical depth, $PM_{2.5}$ and chronic coronary heart disease. Int. J. Health Geogr. 12 (8), 27.
Huang, X., Yang, P., Kattawar, G., Liou, K.-N., 2015. Effect of mineral dust aerosol aspect ratio on polarized reflectance. J. Quant. Spectrosc. Radiat. Transf. 151, 97–109.
Huang, J., Kondragunta, S., Laszlo, I., Liu, H., Remer, L.A., Zhang, H., Petrenko, M., 2016. Validation and expected error estimation of Suomi-NPP VIIRS aerosol optical thickness and Ångström exponent with AERONET. J. Geophys. Res. Atmos. 121 (12), 7139–7160.
Jackson, J.M., Liu, H., Laszlo, I., Kondragunta, S., Remer, L.A., Huang, J., Huang, H.C., 2013. Suomi-NPP VIIRS aerosol algorithms and data products. J. Geophys. Res. Atmos. 118 (22), 12673–12689.
Jiménez, E., Linares, C., Martínez, D., Díaz, J., 2010. Role of Saharan dust in the relationshipbetween particulate matter and short-term daily mortality among the elderly in Madrid (Spain). Sci. Total Environ. 408 (23), 5729–5736.
Kahn, R.A., Gaitley, B.J., 2015. An analysis of global aerosol type as retrieved by MISR. J. Geophys. Res. Atmos. 120 (9), 4248–4281.
Kahn, R., West, R., McDonald, D., Rheingans, B., Mishchenko, M., 1997. Sensitivity of multi-angle remote sensing observations to aerosol sphericity. J. Geophys. Res. 102, 16861–16870.
Kahn, R., Banerjee, P., McDonald, D., Diner, D.J., 1998. Sensitivity of multiangle imaging to aerosol optical depth and to pure-particle size distribution and composition over ocean. J. Geophys. Res. Atmos. 103 (D24), 32195–32213.
Kahn, R.A., Banerjee, P., McDonald, D., 2001. Sensitivity of multi-angle imaging to natural mixtures of aerosols over ocean. J. Geophys. Res. 106, 18219–18238.
Kahn, R.A., Gaitley, B.J., Garay, M.J., Diner, D.J., Eck, T.F., Smirnov, A., Holben, B.N., 2010. Multiangle imaging spectroradiometer global aerosol product assessment by comparison with the Aerosol Robotic Network. J. Geophys. Res. Atmos. 115 (D23), 1–28.
Kaskaoutis, D.G., Kumar, S., Sharma, D., Singh, R.P., Kharol, S.K., Sharma, M., Singh, A.K., Singh, S., Singh, A., Singh, D., 2014. Effects of crop residue burning on aerosol properties, plume characteristics, and long-range transport over northern India. J. Geophys. Res. Atmos. 119, 5424–5444.
Kaufman, Y.J., Tanré, D., Remer, L.A., Vermote, E.F., Chu, A., Holben, B.N., 1997. Operational remote sensing of tropospheric aerosol over land from EOS moderate resolution imaging spectroradiometer. J. Geophys. Res. 102 (D14), 17051–17067.
Kittaka, C., Winker, D.M., Vaughan, M.A., Omar, A., Remer, L.A., 2011. Intercomparison of column aerosol optical depths from CALIPSO and MODIS-Aqua. Atmos. Meas. Tech. 4 (2), 131–141.
Kokhanovsky, A., de Leeuw, G. (Eds.), 2009. Satellite Aerosol Remote Sensing Over Land. Springer, p. 388. ISBN 978-3-540-69396-3.
Kotchenova, S.Y., Vermote, E.F., 2007. Validation of a vector version of the 6S radiative transfer code for atmospheric correction of satellite data. Part II. Homogeneous Lambertian and anisotropic surfaces. Appl. Optics 46 (20), 4455–4464.
Krüger, O., Graßl, H., 2004. Albedo reduction by absorbing aerosols over China. Geophys. Res. Lett. 31 (2). L02108.
Kumar, N., Chu, A., Foster, A., 2007. An empirical relationship between $PM_{2.5}$ and aerosol optical depth in Delhi Metropolitan. Atmos. Environ. 41 (21), 4492–4503.
Kumar, R., Barth, M.C., Pfister, G.G., Naja, M., Brasseur, G.P., 2014. WRF-Chem simulations of a typical pre-monsoon dust storm in northern India: influences on aerosol optical properties and radiation budget. Atmos. Chem. Phys. 14, 2431–2446.
Kumar, M., Singh, R.S., Banerjee, T., 2015a. Associating airborne particulates and human health: exploring possibilities. Environ. Int. 84, 201–202.
Kumar, M., Tiwari, S., Murari, V., Singh, A.K., Banerjee, T., 2015b. Wintertime characteristics of aerosols at middle Indo-Gangetic plain: impacts of regional meteorology and long range transport. Atmos. Environ. 104, 162–175.

Kumar, M., Singh, R.K., Murari, V., Singh, A.K., Singh, R.S., Banerjee, T., 2016. Fireworks induced particle pollution: a spatio-temporal analysis. Atmos. Res. 180, 78–91.

Kumar, M., Raju, M.P., Singh, R.K., Singh, A.K., Singh, R.S., Banerjee, T., 2017a. Wintertime characteristics of aerosols over middle Indo-Gangetic Plain: Vertical profile, transport and radiative forcing. Atmos. Res. 183, 268–282.

Kumar, M., Raju, M.P., Singh, R.S., Banerjee, T., 2017b. Impact of drought and normal monsoon scenarios on aerosol induced radiative forcing and atmospheric heating rate in Varanasi over middle Indo-Gangetic Plain. J. Aerosol Sci. 113, 95–107.

Lee, K.H., Li, Z., Kim, Y.J., Kokhanovsky, A., 2009. Atmospheric aerosol monitoring from satellite observations : a history of three decades. Atmos. Biol. Environ. Monit. 13–38.

Levy, R.C., Remer, L.A., Dubovik, O., 2007. Global aerosol optical properties and application to moderate resolution imaging spectroradiometer aerosol retrieval over land. J. Geophys. Res. 112 (D13), 13210.

Levy, R.C., Mattoo, S., Munchak, L.A., Remer, L.A., Sayer, A.M., Patadia, F., Hsu, N.C., 2013. The Collection 6 MODIS aerosol products over land and ocean. Atmos. Meas. Tech. 6 (11), 2989–3034.

Liu, H., Remer, L.A., Huang, J., Huang, H.-C., Kondragunta, S., Laszlo, I., Jackson, J.M., 2014. Preliminary evaluation of S-NPP VIIRS aerosol optical thickness. J. Geophys. Res. Atmos. 119 (7), 3942–3962.

Lyons, W.A., Husar, R.B., 1976. SMS/GOES visible images detect a synoptic-scale air pollution episode. Mon. Weather Rev. 104, 1623–1626.

Mamun, M.I., Islam, M., Mondol, P.K., 2014. The seasonal variability of aerosol optical depth over Bangladesh based on satellite data and HYSPLIT model. Am. J. Remote Sens. 2 (4), 20–29.

Martinez-Lozano, J.A., Utrillas, M.P., Tena, F., Cachorro, V.E., 1998. The parameterization of the atmospheric aerosol optical depth using the Angstrom power law. Sol. Energy 63, 303–311.

Mazzoni, D., Logan, J.A., Diner, D., Kahn, R., Tong, L., Li, Q., 2007. A data-mining approach to associating MISR smoke plume heights with MODIS fire measurements. Remote Sens. Environ. 107, 138–148.

Mehta, M., 2015. A study of aerosol optical depth variations over the Indian region using thirteen years (2001–2013) of MODIS and MISR Level 3 data. Atmos. Environ. 109, 161–170.

Mehta, M., Singh, R., Singh, A., Singh, N., Anshumali, 2016. Recent global aerosol optical depth variations and trends—a comparative study using MODIS and MISR level 3 datasets. Remote Sens. Environ. 181, 137–150.

Meng, F., Cao, C., Shao, X., 2015. Spatio-temporal variability of Suomi-NPP VIIRS-derived aerosol optical thickness over China in 2013. Remote Sens. Environ. 163, 61–69.

Mishra, A.K., 2014. Retrieval of EVI from Oceansat 2 data and comparison with MODIS derived EVI. J. Indian Soc. Remote Sens. 42 (4), 877–883.

Mishra, A.K., Dadhwal, V.K., 2008. Comparison of enhanced vegetation index from IRS-P4 (OCM) and MODIS on Aqua. Int. J. Geoinform. 4 (4), 57–66.

Mishra, A.K., Dadhwal, V.K., Dutt, C.B.S., 2008. Analysis of marine aerosol optical depth retrieved from IRS-P4 OCM sensor and comparison with the aerosol derived from SeaWiFS and MODIS sensor. J. Earth Syst. Sci. 117 (1), 361–373.

Moffet, R.C., Kimberly, P., 2009. In-Situ Measurements of the mixing state an optical properties of soot with implications for radiative forcing estimates. Proc. Natl. Acad. Sci. 106 (29), 11872–11877.

Moreno, T., Kojima, T., Querol, X., Alastuey, A., Amato, F., Gibbons, W., 2012. Natural versus anthropogenic inhalable aerosol chemistry of trans-boundary East Asian atmospheric outflows into western Japan. Sci. Total Environ. 424, 182–192.

Murari, V., Kumar, M., Barman, S.C., Banerjee, T., 2015. Temporal variability of MODIS aerosol optical depth and chemical characterization of airborne particulates in Varanasi, India. Environ. Sci. Pollut. Res. 22, 1329–1343.

Murari, V., Kumar, M., Singh, N., Singh, R.S., Banerjee, T., 2016. Particulate morphology and elemental characteristics: variability at middle Indo-Gangetic plain. J. Atmos. Chem. 73 (2), 165–179.

Murari, V., Kumar, M., Mhawish, A., Barman, S.C., Banerjee, T., 2017. Airborne particulate in Varanasi over middle Indo-Gangetic Plain: variation in particulate types and meteorological influences. Environ. Monit. Assess. https://doi.org/10.1007/s10661-017-5859-9.

Nagamani, P.V., Chauhan, P., Dwivedi, R.M., 2008. Development of chlorophyll-a algorithm for ocean colour monitor onboard OCEANSAT-2 satellite. IEEE Geosci. Remote Sens. Lett. 5 (3), 527–531.

Nayak, S.R., Sarangi, R.K., Rajawat, A.S., 2001. Application of IRS-P4 OCM data to study the impact of cyclone on coastal environment of Orissa. Curr. Sci. 80 (9), 1208–1213.

North, P.R.J., Briggs, S.A., Plummer, S.E., Settle, J.J., 1999. Retrieval of land surface bidirectional reflectance and aerosol opacity from ATSR-2 multiangle imagery. IEEE Trans. Geosci. Remote Sens. 37 (1), 526–537.

Oliva, P., Schroeder, W., 2015. Assessment of VIIRS 375m active fire detection product for direct burned area mapping. Remote Sens. Environ. 160, 144–155.

Omar, A.H., Won, J.G., Winker, D.M., Yoon, S.C., Dubovik, O., McCormick, M.P., 2005. Development of global aerosol models using cluster analysis of Aerosol Robotic Network (AERONET) measurements. J. Geophys. Res. D: Atmos. 110 (10), 1–14.

Ouillon, S., Lucas, Y., Gaggelli, J., 2002. Hyperspectral detection of sand. In: Proc. 7th Int. conf. Remote Sensing for Marine and Coastal Environments, pp. 681–682.

Prasad, A.K., Singh, R.P., 2007. Changes in aerosol parameters during major dust storm events (2001–2005) over the Indo-Gangetic Plains using AERONET and MODIS data. J. Geophys. Res 112 (D9), 1–18.

Qi, Y., Ge, J., Huang, J., 2013. Spatial and temporal distribution of MODIS and MISR aerosol optical depth over northern China and comparison with AERONET. Chin. Sci. Bull. 58 (20), 2497–2506.

Ramachandran, S., Kedia, S., Srivastava, R., 2012. Aerosol optical depth trends over different regions of India. Atmos. Environ. 49, 338–347.

Raman, R.S., Ramachandran, S., Kedia, S., 2011. A methodology to estimate source-specific aerosol radiative forcing. J. Aerosol Sci. 42 (5), 305–320.

Ramana, M.V., Ramanathan, V., Feng, Y., Yoon, S.-C., Kim, S.-W., Carmichael, G.R., Schauer, J.J., 2010. Warming influenced by the ratio of black carbon to sulphate and the black-carbon source. Nat. Geosci. 3, 542–545.

Ramanathan, V., Ramana, M.V., 2005. Persistent, widespread and strongly absorbing haze over the Himalayan foot hills and the Indo-Gangetic plains,. Pure Appl. Geophys. 162, 1609–1626.

Ramaswamy, V., et al., 2001. Radiative forcing of climate change. Climate Change 2001: The Scientific Basis, Contribution of Working Group I to The Third Assessment Report of The Intergovernmental Panel on Climate Change. Cambridge University Press, New York, NY. pp. 349–416.

Rastogi, N., Singh, A., Sarin, M.M., Singh, D., 2016. Temporal variability of primary and secondary aerosols over northern India: impact of biomass burning emissions. Atmos. Environ. 125, 396–403.

Remer, L.A., Kleidman, R.G., Levy, R.C., Kaufman, Y.J., Tanré, D., Mattoo, S., Martins, J.V., Ichoku, C., Koren, I., Yu, H., Holben, B.N., 2008. Global aerosol climatology from the MODIS satellite sensors. J. Geophys. Res. Atmos. 113 (D14), 1–18.

Remer, L.A., Mattoo, S., Levy, R.C., Munchak, L.A., 2013. MODIS 3 km aerosol product: algorithm and global perspective. Atmos. Meas. Tech. 6 (7), 1829–1844.

Robles Gonzales, C., Veefkind, J.P., De Leeuw, G., 2000. Aerosol optical depth over Europe in August 1997 derived from ATSR-2 data. Geophys. Res. Lett. 27 (7), 955–958.

Robles-Gonzalez, C., De Leeuw, G., Decae, R., Kusmierczyk-Michulec, J., Stammes, P., 2006. Aerosol properties over the Indian Ocean Experiment (INDOEX) campaign area retrieved from ATSR-2. J. Geophys. Res. Atmos. 111 (D15), 1–10.

Satheesh, S.K., Torres, O., Remer, L.A., Babu, S.S., Vinoj, V., Eck, T.F., Holben, B.N., 2009. Improved assessment of aerosol absorption using OMI-MODIS joint retrieval. J. Geophys. Res. Atmos. 114, 1–10.

Sayer, A.M., Hsu, N.C., Bettenhausen, C., Jeong, M.J., 2013. Validation and uncertainty estimates for MODIS Collection 6 "Deep Blue" aerosol data. J. Geophys. Res. Atmos. 118 (14), 7864–7872.

Sayer, A.M., Munchak, L.A., Hsu, N.C., Levy, R.C., Bettenhausen, C., Jeong, M.-J., 2014. MODIS Collection 6 aerosol products: comparison between Aqua's e-Deep Blue, Dark Target, and "merged" data sets, and usage recommendations. J. Geophys. Res. Atmos. 119, 13965–13989.

Schwartz, S.E., Andreae, M.O., 1996. Uncertainty in climate change caused by aerosols. Science 272, 1121–1122.

Sen, A., Ahammed, Y.N., Arya, B.C., Banerjee, T., et al., 2014. Atmospheric fine and coarse mode aerosols at different environments of India and the Bay of Bengal during winter-2014: implications of a coordinated campaign. MAPAN J. Metrol. Soc. India 29 (4), 273–284.

Sen, A., Ahammed, Y.N., Banerjee, T., Chatterjee, A., Choudhuri, A.K., Das, T., Deb, N.C., Dhir, A., Goel, S., Khan, A.H., Mandal, T.K., 2016. Spatial variability in ambient atmospheric fine and coarse mode 20 aerosols over Indo-Gangetic plains, India and adjoining oceans during the onset of summer monsoons, 2014. Atmos. Pollut. Res. 7 (3), 521–532.

Sen, A., Abdelmaksoud, A.S., Ahammed, Y.N., Banerjee, T., Bhat, M.A., Chatterjee, A., Choudhuri, A.K., Das, T., Dhir, A., Dhyani, P.P., Gadi, R., 2017. Variations in particulate matter over Indo-Gangetic Plains and Indo-Himalayan Range during four field campaigns in winter monsoon and summer monsoon: role of pollution pathways. Atmos. Environ. 154, 200–224.

Sharma, A.R., Kharol, S.K., Badarinath, K.V.S., Singh, D., 2010. Impact of agriculture crop residue burning on atmospheric aerosol loading—a study over Punjab State, India. Ann. Geophys. Atmos. Hydrospheres Space Sci. 28 (2), 367–379.

Sharma, M., Kaskaoutis, D.G., Singh, R.P., Singh, S., 2014. Seasonal variability of atmospheric aerosol parameters over Greater Noida using ground sunphotometer observations. Aerosol Air Qual. Res. 14 (3), 608–622.

Shukla, K., Srivastava, P.K., Banerjee, T., Aneja, V.P., 2017. Variation of ground-level and columnar ozone at middle Indo-Gangetic Plain: impacts of seasonality and precursor gases. Environ. Sci. Pollut. Res. 24 (1), 164–179.

Singh, N., Murari, V., Kumar, M., Barman, S.C., Banerjee, T., 2017a. Fine particulates over South Asia: review and meta-analysis of PM 2.5 source apportionment through receptor model. Environ. Pollut. 223, 121–136.

Singh, N., Mhawish, A., Deboudt, K., Singh, R.S., Banerjee, T., 2017b. Organic aerosols over Indo-Gangetic

Plain: sources, distributions and climatic implications. Atmos. Environ. 157, 59–74.
Srivastava, P., Dey, S., Agarwal, P., Basil, G., 2014. Aerosol characteristics over Delhi national capital region: a satellite view. Int. J. Remote Sens. 35 (13), 5036–5052.
Tanré, D., Kaufman, Y.J., Herman, M., Mattoo, S., 1997. Remote sensing of aerosol properties over oceans using the MODIS/EOS spectral radiances. J. Geophys. Res. Atmos. 102 (D14), 16971–16988.
Tanré, D., Bréon, F.M., Deuzé, J.L., Dubovik, O., Ducos, F., François, P., Waquet, F., 2011. Remote sensing of aerosols by using polarized, directional and spectral measurements within the A-Train: the PARASOL mission. Atmos. Meas. Tech. 4 (7), 1383–1395.
Tiwari, S., Singh, A.K., 2013. Variability of aerosol parameters derived from ground and satellite measurements over Varanasi located in the Indo-Gangetic Basin. Aerosol Air Qual. Res. 13, 627–638.
Tiwari, S., Srivastava, A.K., Singh, A.K., Singh, S., 2015. Identification of aerosol types over Indo-Gangetic Basin: implications to optical properties and associated radiative forcing. Environ. Sci. Pollut. Res. 22 (16), 12246–12260.
Todd, W.J., George, A.J., Bryant, N.A., 1979. Satellite-aided evaluation of population exposure to air pollution. Environ. Sci. Technol. 13, 970–974.
Torres, O., Tanskanen, A., Veihelmann, B., Ahn, C., Braak, R., Bhartia, P.K., Levelt, P., 2007. Aerosols and surface UV products from ozone monitoring instrument observations: an overview. J. Geophys. Res. Atmos. 112 (D24), 1–14.
Tripathi, S.N., Pattnaik, A., Dey, S., 2007. Aerosol indirect effect over Indo-Gangetic plain. Atmos. Environ. 41 (33), 7037–7047.
Trivitayanurak, W., Palmer, P.I., Barkley, M.P., Robinson, N.H., Coe, H., Oram, D.E., 2012. The composition and variability of atmospheric aerosol over Southeast Asia during 2008. Atmos. Chem. Phys. 12, 1083–1100.
Twomey, S.A., 1959. The nuclei of natural cloud formation. Part II: the supersaturation in natural clouds and the variation of cloud droplet concentrations. Geofisica Pura e Applicata 43, 227–242.
Utrillas, M.P., Pedro's, R., Martinez-Lozano, J.A., Tena, F., 2000. A new method for determining the Angstrom turbidity coefficient from broadband filter measurement. Am. Meteorol. Soc. 39 (6), 863–874.
Vadrevu, K.P., Ellicott, E., Badarinath, K.V.S., Vermote, E., 2011. MODIS derived fire characteristics and aerosol optical depth variations during the agricultural residue burning season, north India. Environ. Pollut. 159 (6), 1560–1569.
van Donkelaar, A., Martin, R.V., Leaitch, W.R., Macdonald, A.M., Walker, T.W., Streets, D.G., Zhang, Q., Dunlea, E.J., Jimenez, J.L., Dibb, J.E., Huey, L.G., Weber, R., Andreae, M.O., 2008. Analysis of aircraft and satellite measurements from the Intercontinental Chemical Transport Experiment (INTEX-B) to quantify long-range transport of East Asian sulfur to Canada. Atmos. Chem. Phys. 8, 2999–3014.
van Donkelaar, A., Martin, R.V., Brauer, M., Boys, B.L., 2015. Use of satellite observations for long term exposure assessment of global concentrations of fine particulate matter. Environ. Health Perspect. 123, 135–143.
Veefkind, P., De Leeuw, J., 1998. A new algorithm to determine the spectral aerosol optical depth from satellite radiometer measurements. J. Aerosol Sci. 29 (10), 1237–1248.
Veefkind, J.P., De Leeuw, G., Durkee, P.A., 1998. Retrieval of Aerosol Optical Depth over Land using two-angle view Satellite Radiometry during TARFOX. Geophys. Res. Lett. 25 (16), 3135–3138.
Verma, S., Priyadharshini, B., Pani, S., Kumar, D.B., Faruki, A.R., Bhanja, S.N., Mandal, M., 2016. Aerosol extinction properties over coastal West Bengal Gangetic plain under inter-seasonal and sea breeze influenced transport processes. Atmos. Res. 167, 224–267.
von Hoyningen-Huene, W., Freitag, M., Burrows, J.B., 2003. Retrieval of aerosol optical thickness over land surfaces from top-of-atmosphere radiance. J. Geophys. Res. Atmos. 108 (D9), 4260.
Wang, J., Christopher, S.A., 2003. Intercomparison between satellites derived aerosol optical thickness and PM 2.5 mass: implications for air quality studies. Geophys. Res. Lett. 30, 2095.
Wang, M., Son, S., 2016. VIIRS-derived chlorophyll-a using the ocean color index method. Remote Sens. Environ. 182, 141–149.
Wang, J., Kessner, A., Aegerter, C., Sharma, A., Judd, L., Wardlow, B., You, J., Shulski, M., Irmak, S., Kilic, A., Zeng, J., 2016. A multi-sensor view of the 2012 central plains drought from space. Front. Environ. Sci. 4, 45. https://doi.org/10.3389/fenvs.2016.00045.
Wang, H., Zhang, L., Cao, X., Zhang, Z., Liang, J., 2013. A-train satellite measurements of dust aerosol distributions over northern China. J. Quant. Spectrosc. Radiat. Transf. 122, 170–179.
Winker, D.M., Vaughan, M.A., Omar, A., Hu, Y., Powell, K.A., Liu, Z., Young, S.A., 2009. Overview of the CALIPSO mission and CALIOP data processing algorithms. J. Atmos. Ocean. Technol. 26 (11), 2310–2323.
You, W., Zang, Z., Pan, X., Zhang, L., Chen, D., 2015. Estimating $PM_{2.5}$ in Xi'an, China using aerosol optical depth: a comparison between the MODIS and MISR retrieval models. Sci. Total Environ. 505, 1156–1165.
Youn, D., Park, R.J., Jeong, J.I., Moon, B.K., Yeh, S.W., Kim, Y.H., Woo, J.H., Im, E.G., Jeong, J.H., Lee, S.J.,

Song, C.K., 2011. Impacts of aerosols on regional meteorology due to Siberian forest fires in May 2003. Atmos. Environ. 45, 1407–1412.

Yu, H., Chin, M., Bian, H., Yuan, T., Prospero, J.M., Omar, A.H., Zhang, Z., 2015. Quantification of trans-Atlantic dust transport from seven-year (2007–2013) record of CALIPSO lidar measurements. Remote Sens. Environ. 159, 232–249.

Yu, H., Remer, L.A., Kahn, R.A., Chin, M., Zhang, Y., 2013. Satellite perspective of aerosol intercontinental transport: from qualitative tracking to quantitative characterization. Atmos. Res. 124, 73–100.

Zeeshan, M., Oanh, N.T.K., 2015. Relationship of MISR component AODs with black carbon and other ground monitored particulate matter composition. Atmos. Pollut. Res. 6 (1), 62–69.

Further Reading

Bellouin, N., Boucher, O., Tanré, D., Dubovik, O., 2003. Aerosol absorption over the clear-sky oceans deduced from POLDER-1 and AERONET observations. Geophys. Res. Lett. 30 (14), 1748.

Deuzé, J.L., Bréon, F.M., Devaux, C., Goloub, P., Herman, M., Lafrance, B., Tanré, D., 2001. Remote sensing of aerosols over land surfaces from POLDER-ADEOS-1 polarized measurements. J. Geophys. Res. Atmos. 106 (D5), 4913–4926.

Duncan, B.N., Prados, A.I., Lamsal, L.N., 2014. Satellite data of atmospheric pollution for U.S. air quality applications: examples of applications, summary of data end-user resources, answers to FAQs, and common mistakes to avoid. Atmos. Environ. 94, 647–662.

Kaufman, Y.J., Koren, I., Remer, L.A., Tanre, D., Ginoux, P., Fan, S., 2005. Dust transport and deposition observed from the Terra-Moderate Resolution Imaging Spectroradiometer (MODIS) spacecraft over the Atlantic Ocean. J. Geophys. Res. 110, D10S12.

Mekler, Y., Quenzel, H., Ohring, G., Marcus, I., 1977. Relative atmospheric aerosol content from ERS observations. J. Geophys. Res. 82, 967–972.

Muhammad, Z., Oanh, K.N., 2015. Relationship of MISR component AODs with black carbon and other ground monitored particulate matter composition. Atmos. Pollut. Res. 6 (1), 62–69.